NANOTECHNOLOGY: BEYOND IMAGINATION

PRESENTED BY:
PROF. S. Y. MENSAH
F.A.A.S; F.G.A.A.S

UNIVERSITY OF CAPE COAST, GHANA.

Presentation Outline

The presentation will take the following form:

- *Who is a theoretical Physicist ?*
- *What is the difference between a theoretical and experimental physicist and why is there a difference?*
- *A brief introduction to Nanotechnology*
- *An overview of Carbon Nanotube*
- *Application of Nanotechnology*
- *Thermoelectric Figure of Merit of Chiral Carbon Nanotube*
- *Conclusion*

Who is a theoretical Physicist ?

- Theoretical physics employs mathematical models and abstractions of physics in an attempt to explain natural phenomena in a mathematical form. Its central core is mathematical physics, though other conceptual techniques are also used. ...
  en.wikipedia.org/wiki/Theoretical_physics
- · the description of natural phenomena in mathematical form, especially in order to derive fundamental laws of nature and to derive conclusions ...
  en.wiktionary.org/wiki/theoretical_physics

European Organization for Nuclear Research

- Theoretical physicists are rather typical scientists. If you imagine them as absent-minded, egg-headed, bizarre characters scratching their chins while deeply engaged in thought... Well, most of the time you'd be right.
- What this people do is to try to figure out how Nature works. That is, why the stars shine, why water is fluid and the sky is blue, what you are made of and why does "it" weigh that much, why the universe expands, or what energy and matter actually ARE…

by Alvaro de Rújula

- source: http://public.web.cern.ch/public/en/People/People-en.html

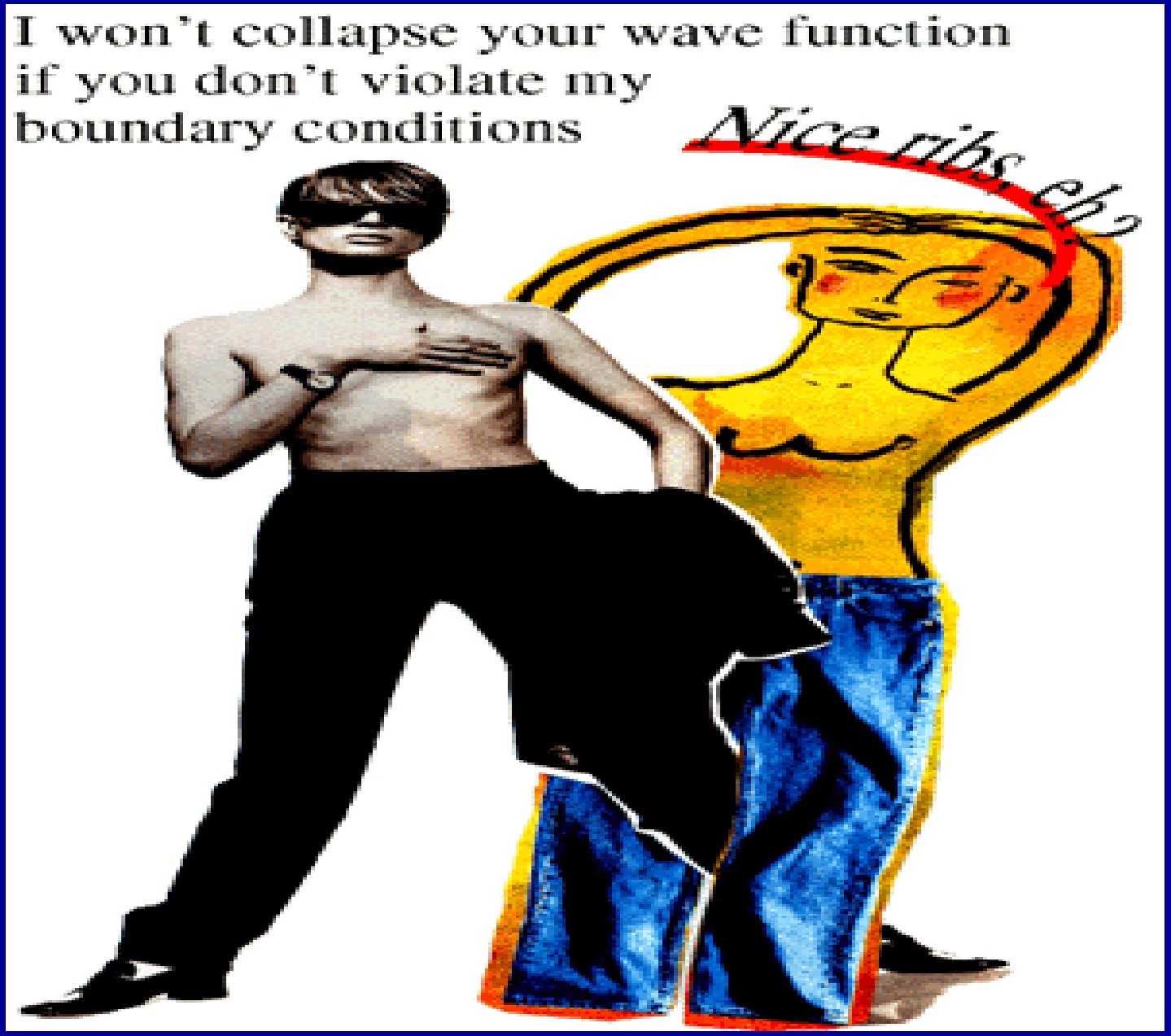
I won't collapse your wave function
if you don't violate my
boundary conditions
Nice ribs, eh?

what is the difference between a theoretical and an experimental physicist and why is there a difference?"

- The answer to the second question is simple: the two "species" do quite different and often very specialized things. It is increasingly hard to find people like Leonardo da Vinci, who know and are active on "everything". The experimentalist interrogates Nature directly, by observing it passively, like astronomers do, or actively, like particle experimentalists do, in "playing" with Nature's smallest constituents to figure out directly how they behave.
- The relation between experimentalists and theorists is often one of healthy competition for truth and less healthy competition for fame. Here is a riddle reflecting that fact:
- What is similar and what is different between the following two sets?:

- The first set consists of a farmer, his pig and the truffles(edible fungi)

- The second set consists of the theorist, the experimentalist and the big discoveries

(you can see by my drawing of the second set that I am not an experimentalist).

- The answer to the riddle is:
- The farmer takes his pig to the woods. The pig snifs around looking for a truffle. When the pig gets it and is about to eat it, the farmer kicks the pig on the head with his club and steals the truffle. Those are the similarities: a theorist would also claim recognition for an experimenter's discovery (if it has anything to do with her/his theories) even if [s]he did not make it!

- The difference is that the farmer always takes the pig to woods where there are truffles, while more often than not, the suggestions by the theorists take the experimentalists to "woods" where there are no "truffles" (by suggesting experiments that do not lead to interesting discoveries).

Theoretical physicists 1

2 Principle of the experiment

Applying an ac field to a superlattice results in IV characteristics that look quite different in the presence and in the absence of domains. First, we consider the case of a low-frequency ac field. Miniband transport theory, formulated without an account of domain formation, predicts that in the limit $\omega\tau \ll 1$ an application of an ac field results in a shift of the maximum of the IV curve towards larger voltages in comparison with the nonirradiated superlattice [21, 22]. This "right shift" is caused by a nonlinearity of the Esaki-Tsu characteristic: the shift increases

References

1. L. Esaki, R. Tsu, IBM J. Res. Dev. **14**, 61 (1970)
2. M. Büttiker, H. Thomas, Phys. Rev. Lett. **38**, 78 (1977)
3. H. Le Person, C. Minot, L. Boni, J.F. Palmier, F. Mollot, Appl. Phys. Lett. **60**, 2397 (1992)

20. T.Ya. Banis, I.V. Parshelyunas, Yu.K. Pozhela, Lietuvos Fiz. Rink. (Lithuanian Phys. J.) **11**, 1013 (1971)
21. S.Y. Mensah, J. Phys.: Condens. Matter **4**, L325 (1992)
22. A.A. Ignatov, Yu.A. Romanov, Izv. VUZ Radiofiz. **21**, 132 (1978) [Radiophysics and Quantum Electronics (Consultants Bureau, New York) **21**, 91 (1978)]

Theoretical physicists 2

Eur. Phys. J. B **39**, 483–489 (2004)
DOI: 10.1140/epjb/e2004-00221-y

THE EUROPEAN PHYSICAL JOURNAL B

Ultrafast creation and annihilation of space-charge domains in a semiconductor superlattice observed by use of Terahertz fields

F. Klappenberger[1,a], K.N. Alekseev[1,b], K.F. Renk[1], R. Scheuerer[1], E. Schomburg[1], S.J. Allen[2], G.R. Rami
J.S.S. Scott[2], A. Kovsh[3], V. Ustinov[3], and A. Zhukov[3]

[1] Institut für Angewandte Physik, Universität Regensburg, 93053 Regensburg, Germany
[2] iQuest, University of California at Santa Barbara, CA 93106-5100, USA
[3] Ioffe Institute, St Petersburg 194021, Russia

Received 25 March 2004
Published online 23 July 2004 – © EDP Sciences, Società Italiana di Fisica, Springer-Verlag 20

Abstract. We report an experimental study indicating ultrafast creation and annihilation of s
domains in a semiconductor superlattice under the action of a THz field. Our experiment w
for an InGaAs/InAlAs superlattice with the conduction electrons undergoing miniband
applied to a superlattice a dc bias that was slightly smaller than a critical bias necessary fo
of space-charge domains caused by a static negative differential conductivity. Additional
superlattice to a strong THz field, resulted in a dc transport governed by the formation
frequency of the field was smaller than an upper frequency limit (~3 THz). From this
the creation and annihilation of domains we determined the characteristic time of
Our analysis shows that the buildup time of domains in a wide miniband and heav
is limited by the relaxation time due to scattering of the miniband electrons a
Our results are of importance for both an understanding of ultrafast dynamics
nanostructures and the development of THz electronic devices.

PACS. 72.20.Ht High-field and nonlinear effects – 72.30.+q High-frequency e
73.21.Cd Superlattices

4 Analysis of the experimental results

For the GaAs/AlAs superlattice, we found $\tau_{diel} \sim$ 340 fs. Because here $\tau_{diel} > T$, the characteristic time of domain formation is determined by τ_{diel}. Thus, for this superlattice τ_{dom} was longer than the half-period already at 2 THz ($T/2 = 250$ fs) resulting in a "right shift" of the IV maximum, which is typical for a superlattice without domain formation (see [2] and Sect. 4.3 below).

Theoretical physicists 3

APPLIED PHYSICS LETTERS VOLUME 73, NUMBER 20 16 NOVEMBER 1998

Ultrafast detection and autocorrelation of picosecond THz radiation pulses with a GaAs/AlAs superlattice

S. Winnerl, W. Seiwerth, E. Schomburg, J. Grenzer, and K. F. Renk[a)]
Institut für Angewandte Physik, Universität Regensburg, Germany

C. J. G. M. Langerak and A. F. G. van der Meer
FOM–Institute for Plasma Physics "Rijnhuizen," Nieuwegein, The Netherlands

D. G. Pavel'ev, Yu. Koschurinov, and A. A. Ignatov
Department of Radiophysics, Nizhny Novgorod State University, Russia

B. Melzer, V. Ustinov, S. Ivanov, and P. S. Kop'ev
Physico-Technical Institute (Ioffe Institute), St. Petersburg, Russia

(Received 20 May 1998; accepted for publication 21 September 1998)

We used a wide miniband GaAs/AlAs superlattice (at room temperature) for detection and autocorrelation of picosecond THz radiation pulses (frequency 4.3 THz) from a free-electron laser. The detection was based on a THz-field induced change in conductivity of the superlattice, and the correlation on the nonlinearity of the conductivity change at strong THz-pulse-power. The nonlinear conductivity change was due to two effects, which we attribute to dynamical localization of miniband electrons and to ionization of deep impurity centers. © *1998 American Institute of Physics.* [S0003-6951(98)04946-8]

A further indication for the presence of deep impurity centers comes from photoluminescence studies (at 77 K) of the superlattice. The photoluminescence spectrum contained a peak at an energy 80 meV below the peak of the lowest miniband. Recently, a theoretical study predicted that the current–voltage characteristic of a superlattice should show, at very strong static fields, an exponential rise of current due to ionization of impurities. A contribution to the current

12

[10] P. M. Mooney, J. Appl. Phys. **67**, R1 (1990).
[11] H. Künzel, K. Ploog, K. Wünstel, and B. L. Zhou, J. Electron. Mater. **13**, 281 (1984).
[12] S. Y. Mensah, F. K. A. Allotey, and A. Clement, Superlattices Microstruct. **19**, 151 (1996).
[13] H.-W. Hübers, G. W. Schwaab, and H. P. Röser, J. Appl. Phys. **75**, 4243 (1994).

12

NANOTECHNOLOGY

- **DEFINITION:**
- **The most common definition of nanoscience is ‘the ability to do things – measure, see, predict and make – on the scale of atoms and molecules and exploit the novel properties found at that scale.**

- What is the scale?

- **Traditionally, this scale is defined as between 0.1 and 100 nanometre (nm).**

Nanotechnology

- **Characterisation of Nanotechnology**

Nanotechnology is characterised by distinguishing between the fabrication processes of top-down and bottom up.

Top-down

Top-down technology refers to the fabrication of nanoscale structures by machining and etching techniques. It is important to note that in miniaturisation at the nanoscale level, quantum laws operate and surface behaviour starts to dominate over the behaviour of bulk materials.

Metal Organic Chemical Vapour Depositon (MOCVD)

Kansas State University

Molecular Beam Epitaxy (MBE)

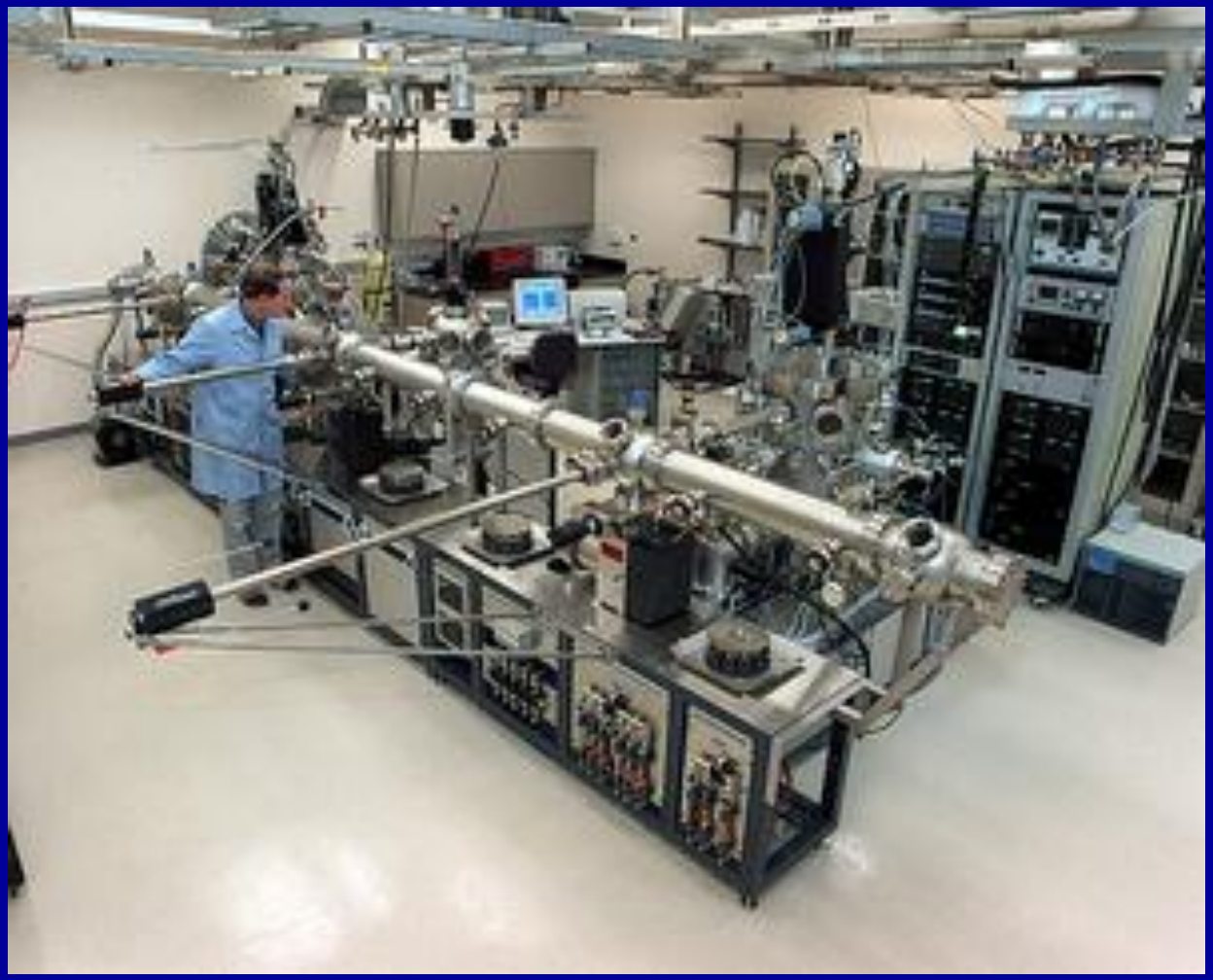

The Molecular Beam Epitaxy System in the William R. Wiley Environmental Molecular Sciences Laboratory.

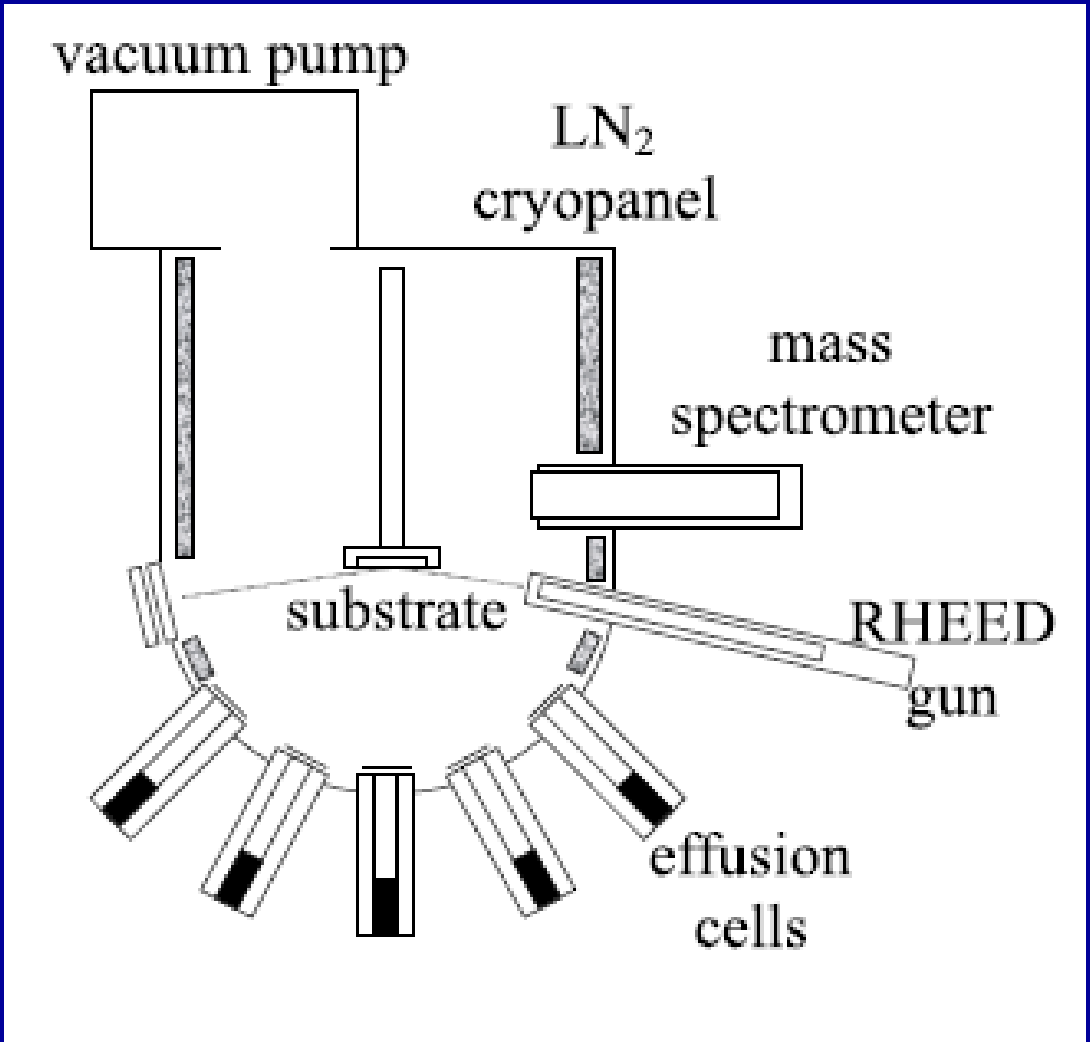

Schematic diagram of a typical MBE

Bottom-up

Bottom-up technology refers to molecular nanotechnology (MNT) which means creation of organic and inorganic structures, atom by atom or molecule by molecule.

Productive Nanosystems:

From molecules to superproducts

Version 1.00

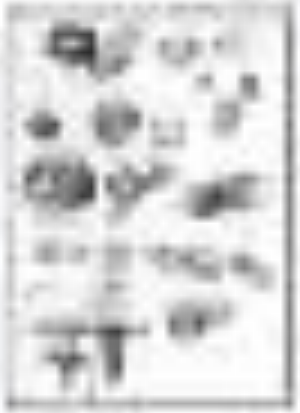

- **What is the situation now?**

- **At present the bottom up is far from realization. Nanotechnology as applied today is mainly top down,**

- **Novel Materials**

- **It is a known fact that material science and technology is fundamental to a majority of the applications of nanotechnology.**

- **Novel materials that can be classified under nanotechnology are the following:**

- Quantum well structures (heterostructures, superlattices, multiple quantum wells and quantum wire)
- Quantum dot structures
- Photonic crystals
- Carbon nanotubes
- Spintronics
- Polymers

SUPERLATTICE

- Superlattice is a periodic structure of repeating quantum wells that sets up a new set of selection rules which affects the conditions for charges to flow through the structure.

- This nanostructure consists of two different semiconductor materials, which are deposited alternately on each other to form a periodic structure in the growth direction. Since the first proposal by Leo Esaki and Raphael Tsu of synthetic artificial superlattices in 1970,[1] great advances in the physics of such ultra-fine semiconductors, presently called quantum structures, have been made within the past two decades.
- The concept of quantum confinement has led to the observation of quantum size effects in isolated quantum well heterostructures and is closely related to superlattices through the tunneling phenomena. Therefore, these two ideas are often discussed on the same physical basis, but each field has its own intrigue and different physics useful for applications in many electric and optical devices.

Schematic representation of superlattice

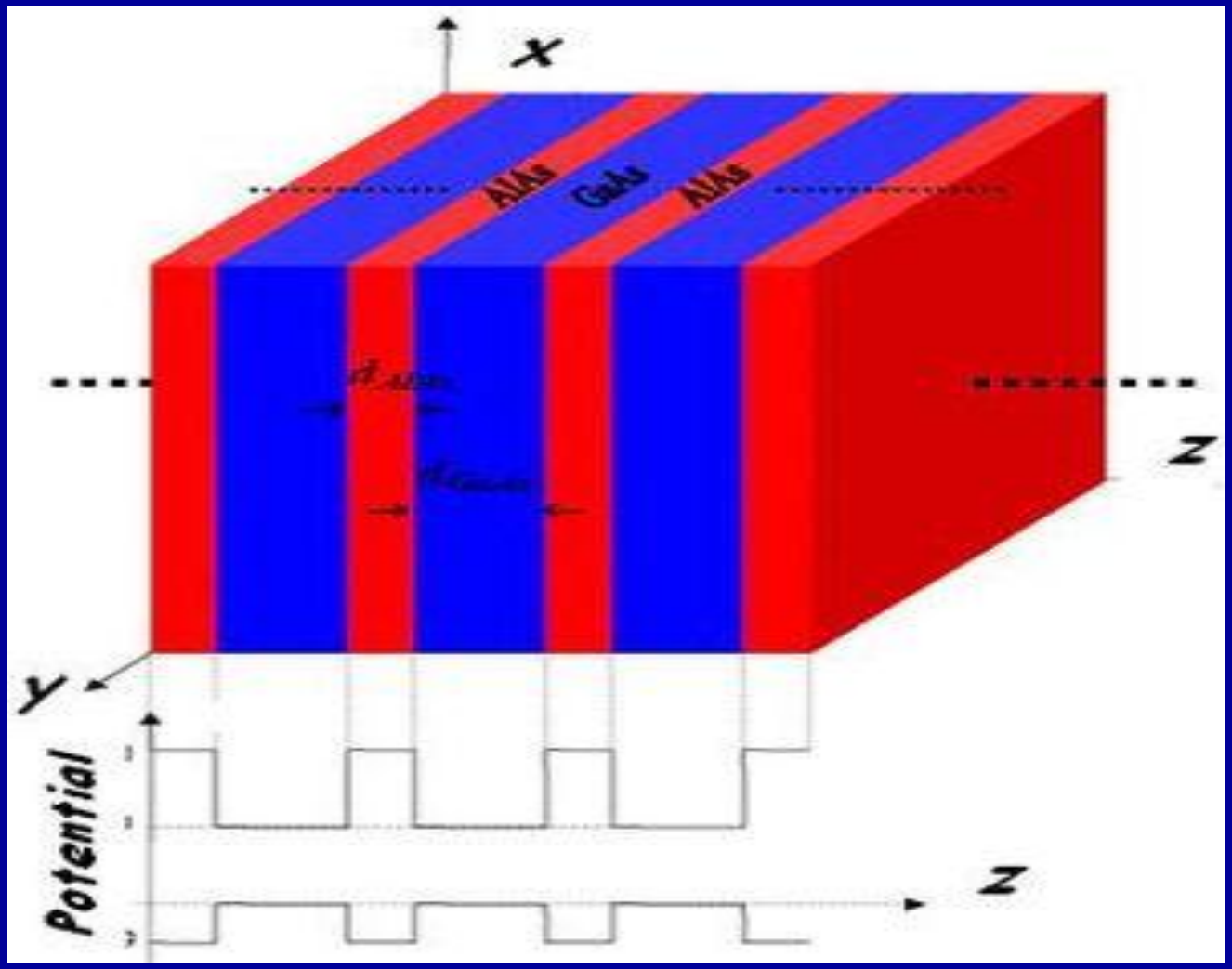

Prof. S.Y. Mensah meets Leo Esaki (Nobel Prize winner 1973)

HETEROJUNCTION

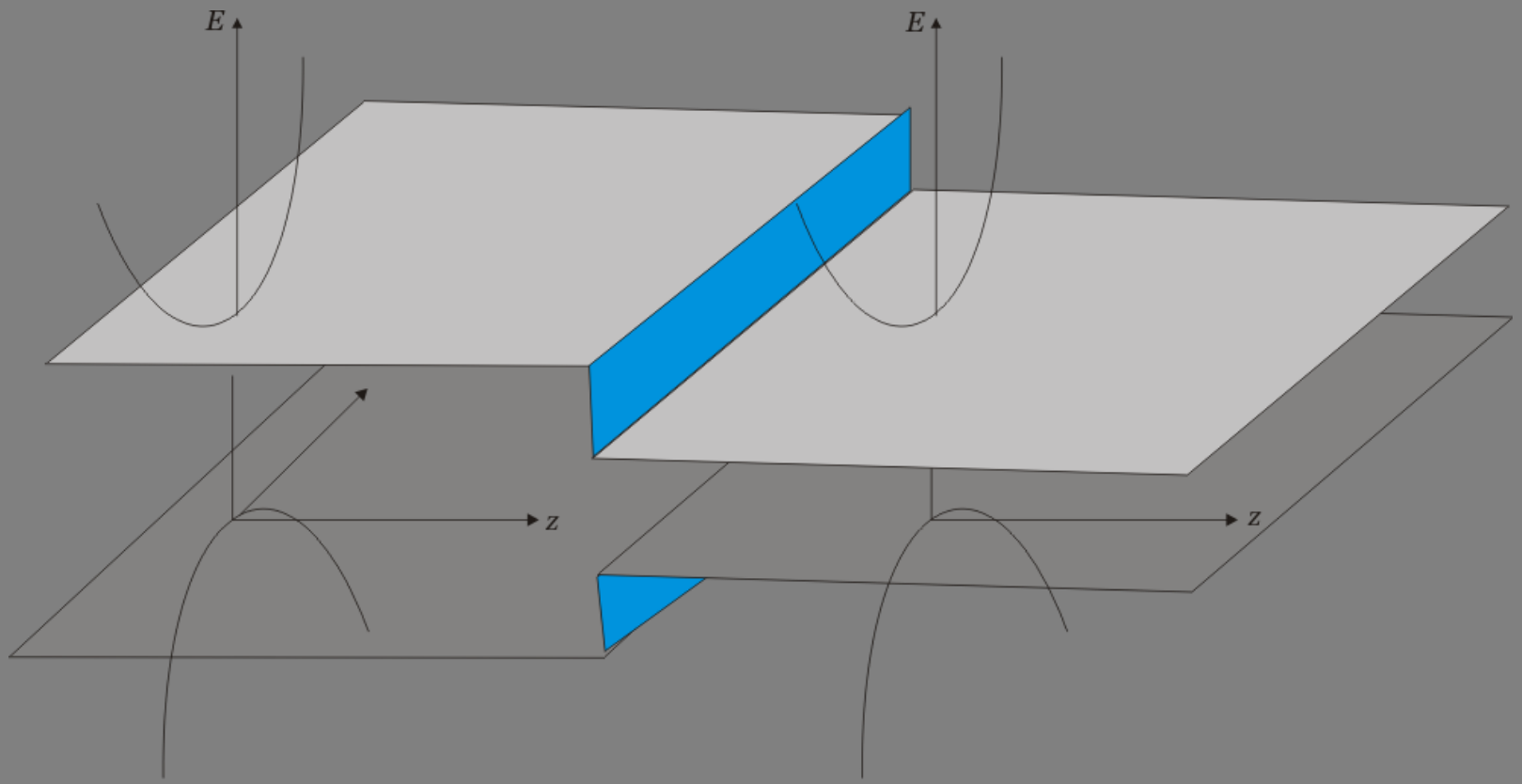

Two dissimilar semiconductors with different bandgaps joined to form a heterojunction; the curves represent the unrestricted motion parallel to the interface

HETEROSTRUCTURES

- Heterostructures are formed from multiple heterojunctions. If a thin layer of a narrower-bandgap material ‘A’ is sandwiched between two layers of wider-bandgap material ‘B’, then they form a double heterojunction.

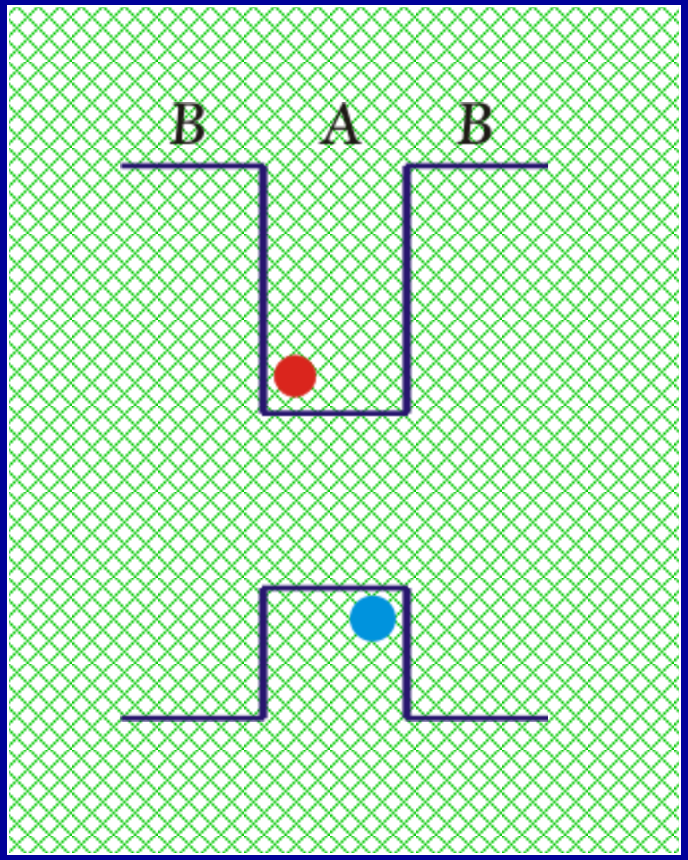
B
A
B

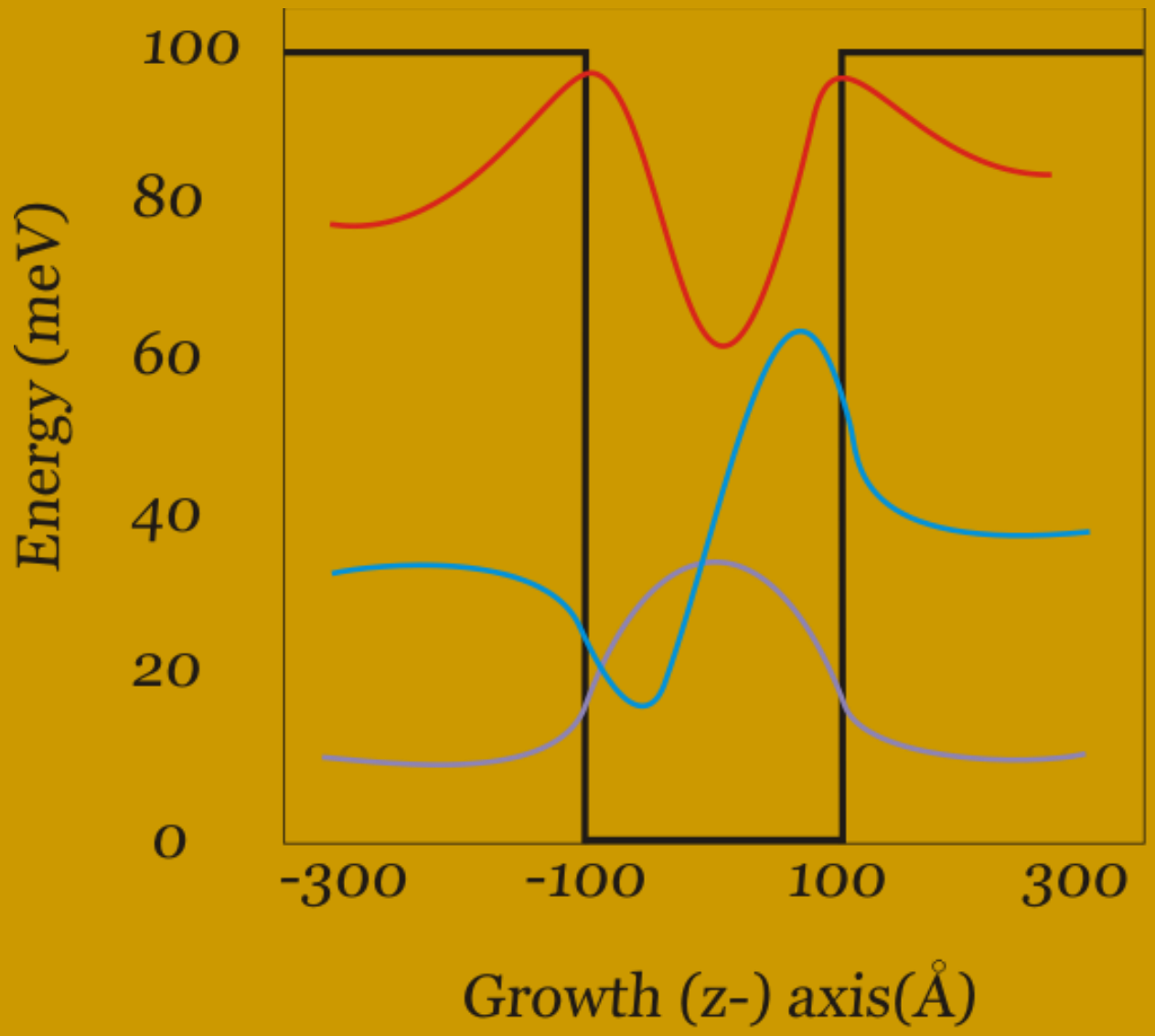

Eigenfunction $\psi(z)$ for the first three energy levels of the 200Å GaAs well

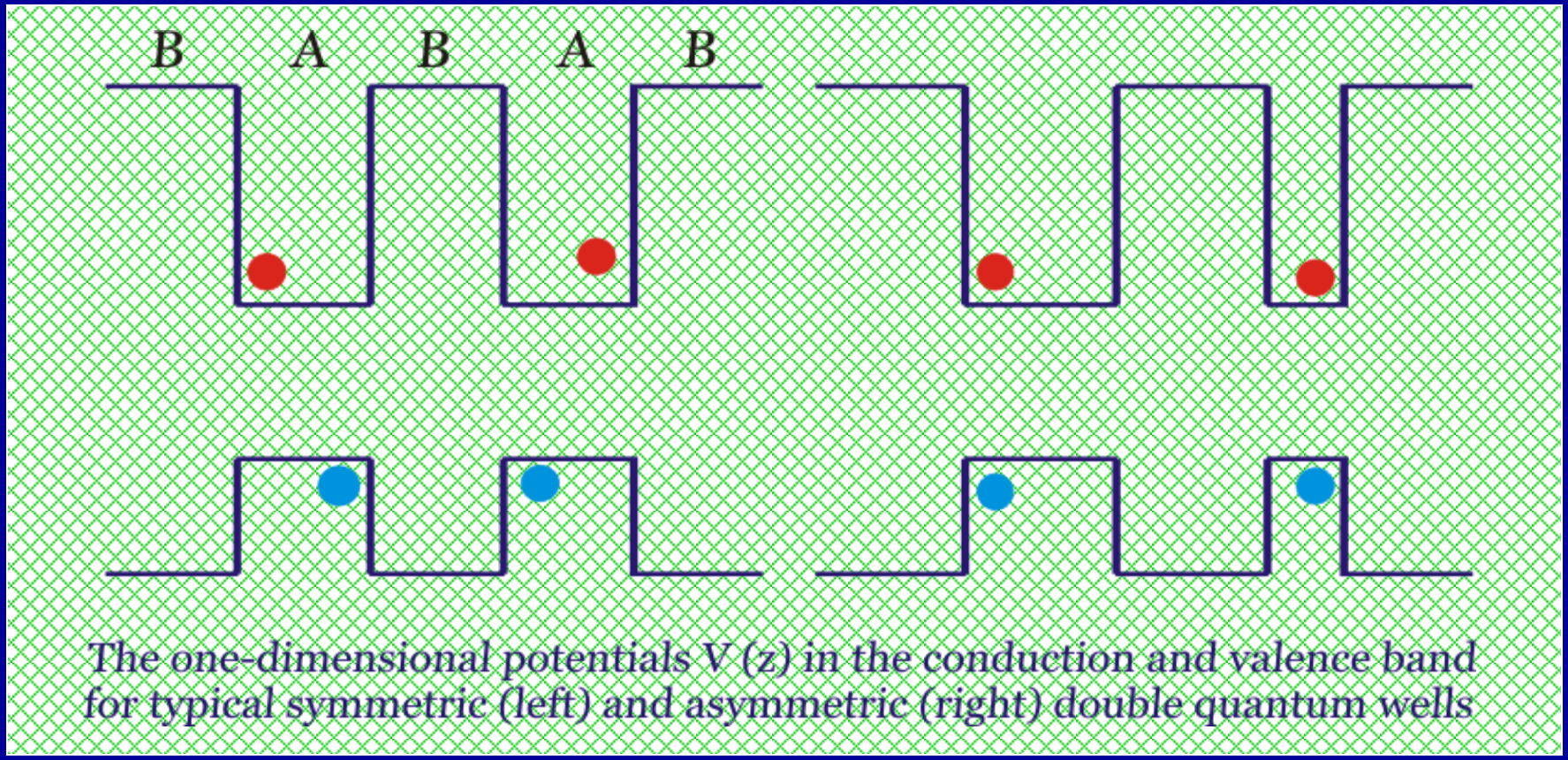

The one-dimensional potentials V (z) in the conduction and valence band for typical symmetric (left) and asymmetric (right) double quantum wells

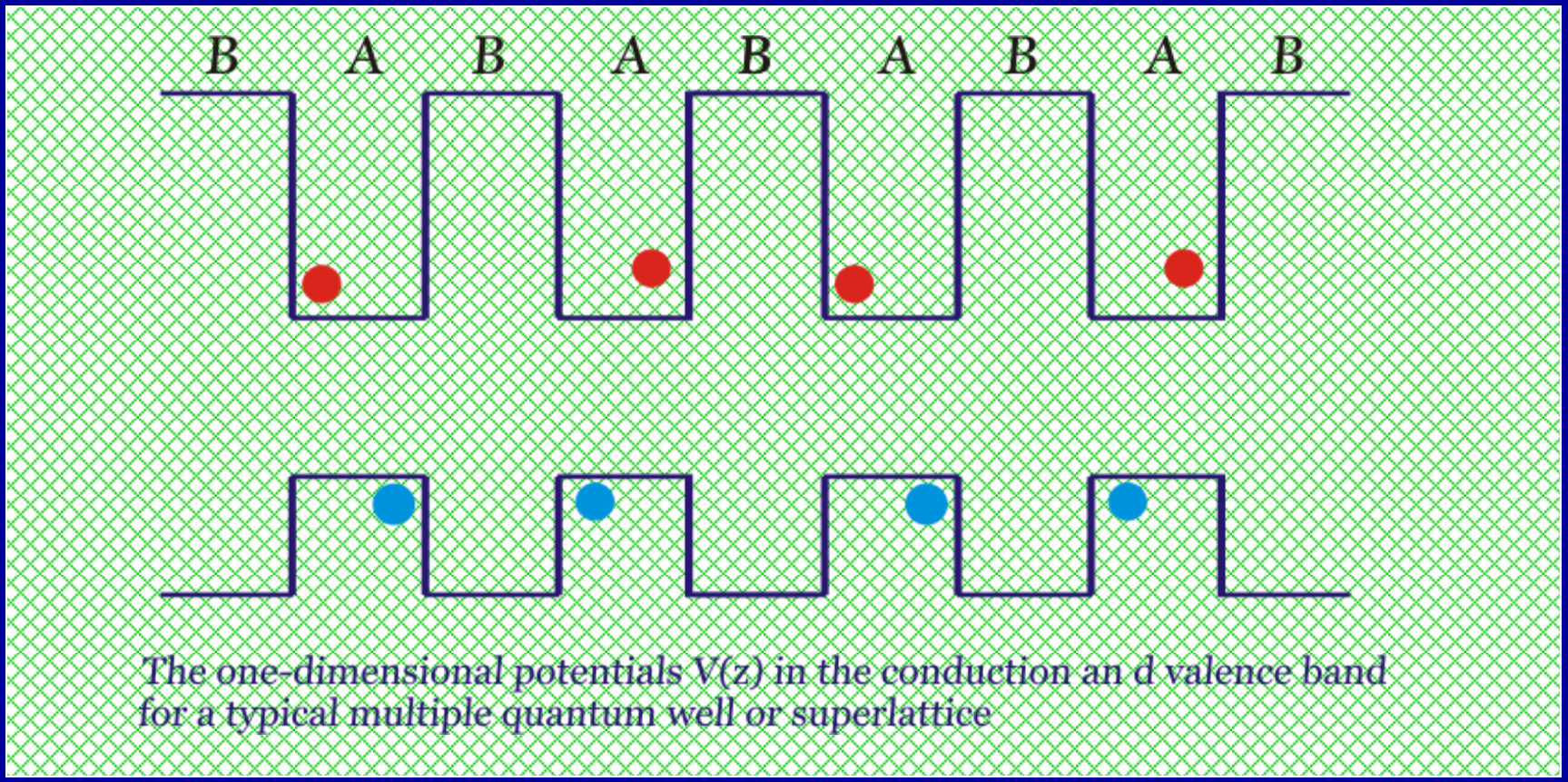

The one-dimensional potentials V(z) in the conduction an d valence band for a typical multiple quantum well or superlattice

CARBON NANOTUBE

Kofi W. Adu

Ph.D.

B.S., Physics, University of Cape Coast, Ghana 1994

(814) 865-0343

cxa269@psu.edu Personal website

EDUCATION

Ph.D., Physics, Pennsylvania State University, University Park, PA, May 2004.

Thesis Title: "Synthesis and Raman Scattering Studies of Novel Semiconductor nanostructures: Si and Ge and GaAs "Twinning Superlattice" Nanowires

B.Sc., Physics, University of Cape Coast, Cape Coast, Ghana, 1994.

Thesis Title: "Effect of Ionization of Impurity Centers by Electric Field on the Conductivity of Superlattice."

- **DISCLOSURES/PATENT APPLICATIONS**
-
- **"Thermoelectric Characterization of Hydrogen Storage in Carbon Nanotubes"** P.C Eklund, G. U. Sumanasekera, **C. Adu,** B. K. Pradhan, Provisional application filed Oct. 2000.
- **"Carbon Nanotubes: A thermoelectric Nano-nose"** P.C Eklund, G. U. Sumanasekera, **K. W. Adu,** B. K. Pradhan, Invention Disclosure # 2000-2357.
- " **Thermal Production of Semiconductor Nanotubes (GaAs nanowires)**", **K. W. Adu,** B. K. Pradhan, P. C. Eklund, Request for provisional application March 2002

www.personal.psu.edu/pce3/group_members/kofi.htm

CARBON NANOTUBE

- Carbon nanotubes (CNTs) are an allotrope of carbon. They take the form of cylindrical carbon molecules and have novel properties that make them potentially useful in a wide variety of applications in nanotechnology, electronics, optics and other fields of materials science. They exhibit extraordinary strength and unique electrical properties, and are efficient conductors of heat. Inorganic nanotubes have also been synthesized.

- Nanotubes are members of the fullerene structural family, which also includes buckyballs. Whereas buckyballs are spherical in shape, a nanotube is cylindrical, with at least one end typically capped with a hemisphere of the buckyball structure. Their name is derived from their size, since the diameter of a nanotube is on the order of a few nanometers (approximately 50,000 times smaller than the width of a human hair), while they can be up to several millimeters in length. There are two main types of nanotubes: single-walled nanotubes (SWNTs) and multi-walled nanotubes (MWNTs).

...DISCOVERY OF CARBON NANOTUBE

- In 1952 Radushkevich and Lukyanovich published clear images of 50 nanometer diameter tubes made of carbon in the Russian *Journal of Physical Chemistry*. This discovery was largely unnoticed; the article was published in the Russian language, and Western scientists' access to Russian press was limited during the Cold War. It is likely that carbon nanotubes were produced before this date, but the invention of the transmission electron microscope allowed the direct visualization of these structures. A 2006 editorial written by Marc Monthioux and Vladimir Kuznetsov in the journal *Carbon* has described the interesting and often misstated origin of the carbon nanotube. A large percentage of academic and popular literature attributes the discovery of hollow, nanometer sized tubes composed of graphitic carbon to Sumio Iijima of NEC in 1991.

Types of Carbon Nanotube

- SINGLE-WALLED

- Most single-walled nanotubes (SWNT) have a diameter of close to 1 nanometer, with a tube length that can be many thousands of times larger. single-walled nanotubes with length up to orders of centimeters have been produced . The structure of a SWNT can be conceptualized by wrapping a one-atom-thick layer of graphite called graphene into a seamless cylinder. The way the graphene sheet is wrapped is represented by a pair of indices (*n*,*m*) called the chiral vector. The integers *n* and *m* denote the number of unit vectors along two directions in the honeycomb crystal lattice of graphene. If *m*=0, the nanotubes are called "zigzag". If *n*=*m*, the nanotubes are called "armchair". Otherwise, they are called "chiral".

Multi-walled

Multiwalled nanotubes (MWNT) consist of multiple layers of graphite rolled in on themselves to form a tube shape. There are two models which can be used to describe the structures of multiwalled nanotubes. In the ***Russian Doll*** model, sheets of graphite are arranged in concentric cylinders, eg a (0,8) single-walled nanotube (SWNT) within a larger (0,10) single-walled nanotube. In the ***Parchment*** model, a single sheet of graphite is rolled in around itself, resembling a scroll of parchment or a rolled up newspaper. The interlayer distance is close to the distance between graphene layers in graphite. The special place of Double-walled Carbon Nanotubes (DWNT) must be emphasized here because they combine very similar morphology and properties as compared to SWNT, while improving significantly their chemical resistance. This is especially important when functionalisation is required (this means grafting of chemical functions at the surface of the nanotubes) to add new properties to the CNT.

•Fullerite

- A fullerite is a highly incompressible nanotube form. Polymerized single walled nanotubes (P-SWNT) are a class of fullerites and are comparable to diamond in terms of hardness. However, due to the way that nanotubes intertwine, P-SWNTs don't have the corresponding crystal lattice that makes it possible to cut diamonds neatly. This same structure results in a less brittle material, as any impact that the structure sustains is spread out throughout the material.

THE STRUCTURE OF THE CARBON NANOTUBE

- Manufacturing a nanotube is dependent on applied quantum mechanics, specifically, orbital hybridization. Nanotubes are composed entirely of sp2 bonds, similar to those of graphite. This bonding structure, which is stronger than the sp3 bonds found in diamond, provides the molecules with their unique strength. Nanotubes naturally align themselves into "ropes" held together by Van der Waals forces. Under high pressure, nanotubes can merge together, trading some sp2 bonds for sp3 bonds, giving great possibility for producing strong, unlimited-length wires through high-pressure nanotube linking.

Hexagonal Lattice (Definition of Vectors)

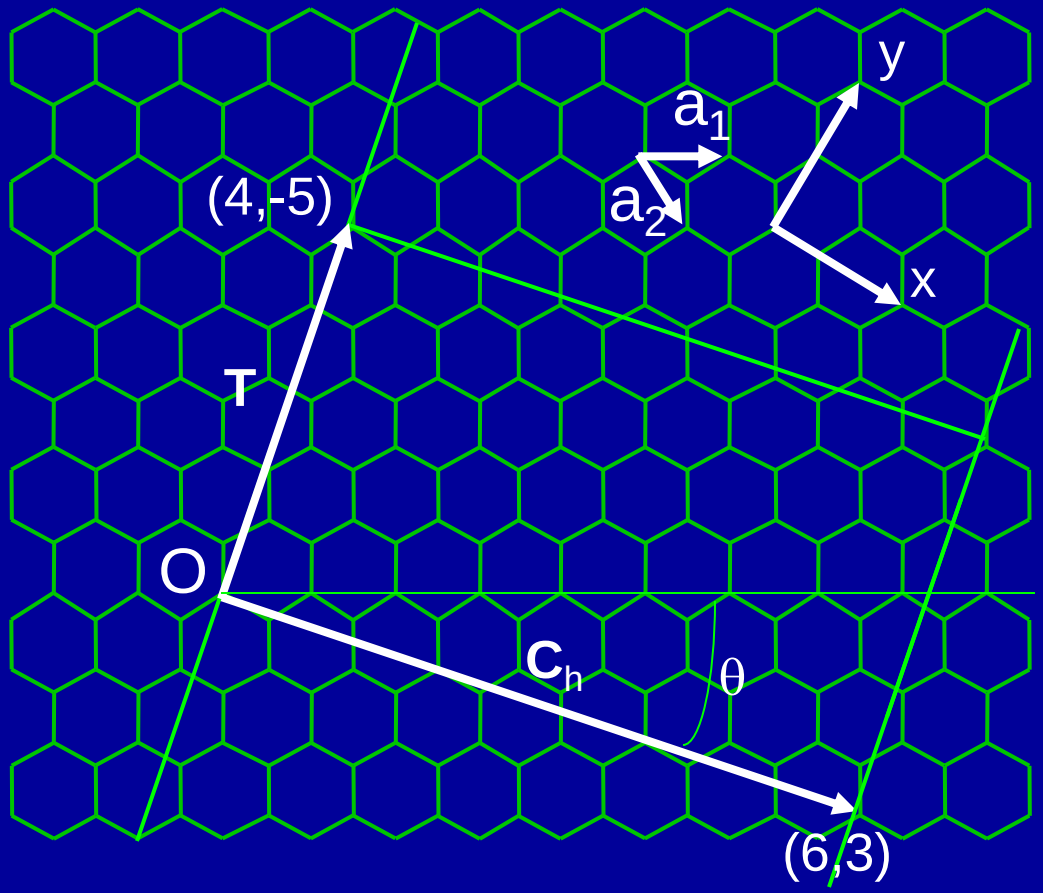

Chiral vector

$$\mathbf{C}_h = n\mathbf{a}_1 + m\mathbf{a}_2$$

$$\mathbf{a}_1 = (\frac{3}{2}a_{cc}, \frac{\sqrt{3}}{2}a_{cc})$$

$$\mathbf{a}_2 = (\frac{3}{2}a_{cc}, -\frac{\sqrt{3}}{2}a_{cc})$$

$$|\mathbf{a}_1| = |\mathbf{a}_2| = \sqrt{3}a_{cc} \equiv a$$

$$\mathbf{a}_1 = (\frac{\sqrt{3}}{2}, \frac{1}{2})a$$

$$\mathbf{a}_2 = (\frac{\sqrt{3}}{2}, -\frac{1}{2})a$$

Wrapping (10,0) SWNT (zigzag)

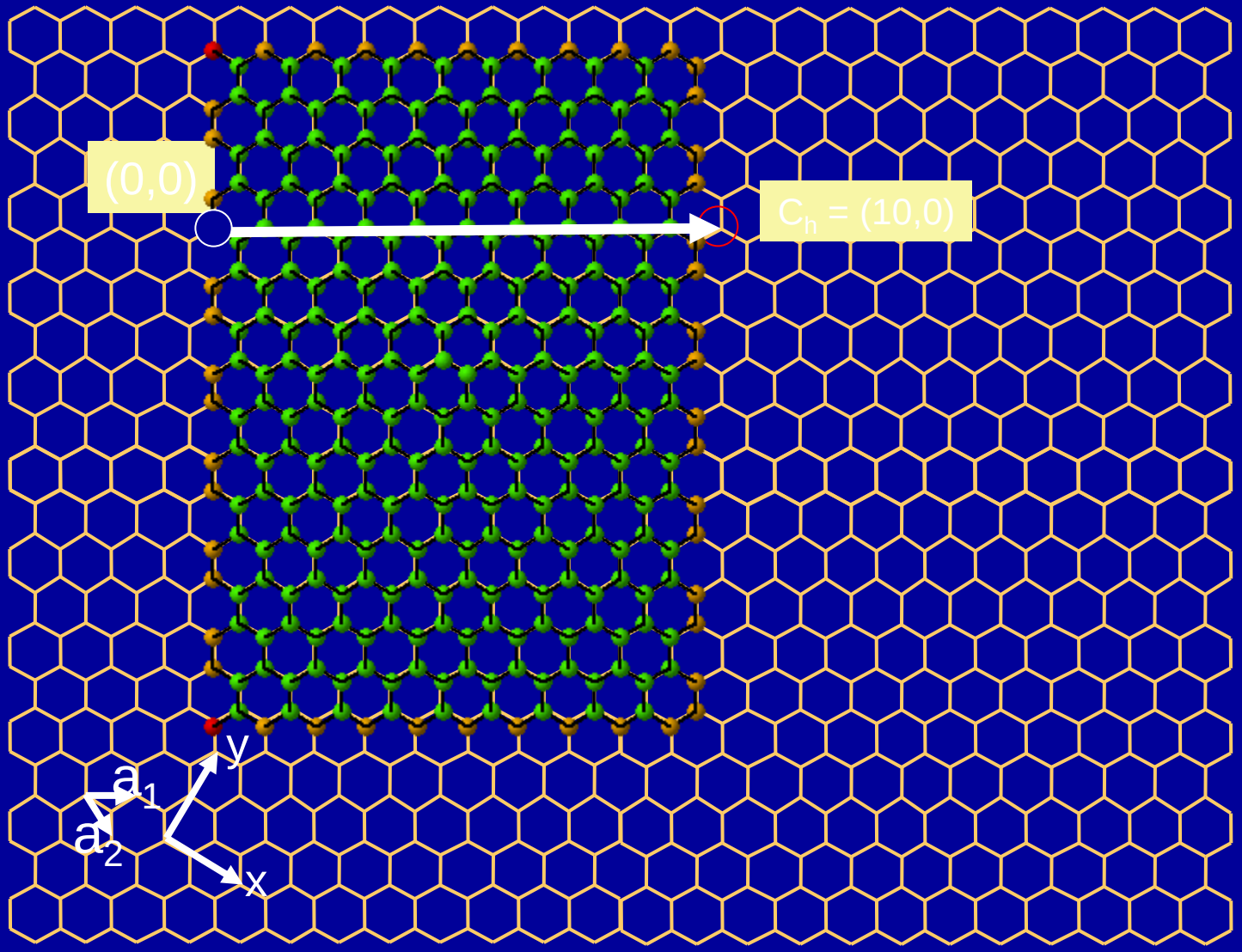

Wrapping (10,0) SWNT (Animation)

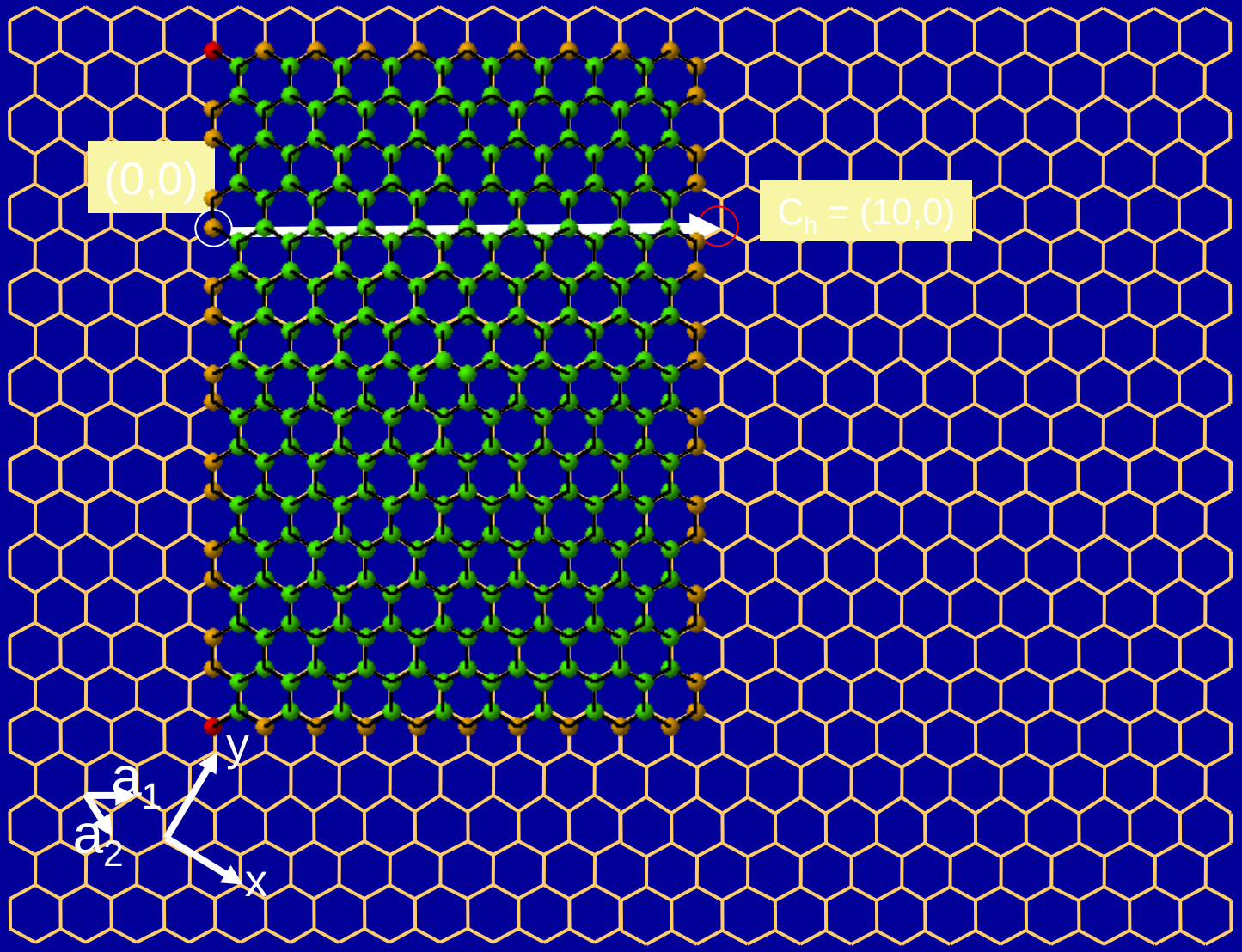

Wrapping (10,10) SWNT (armchair)

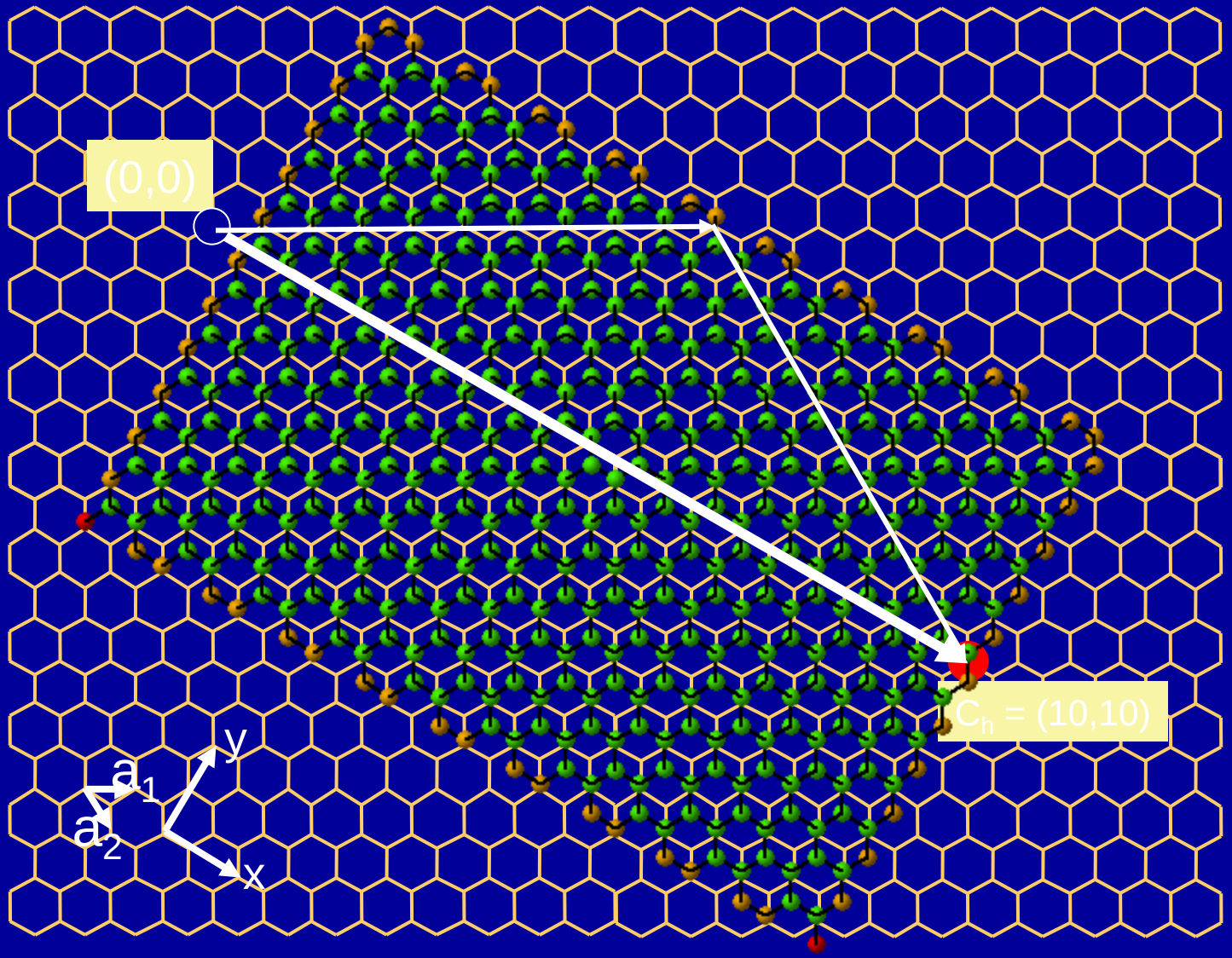

Wrapping (10,10) SWNT

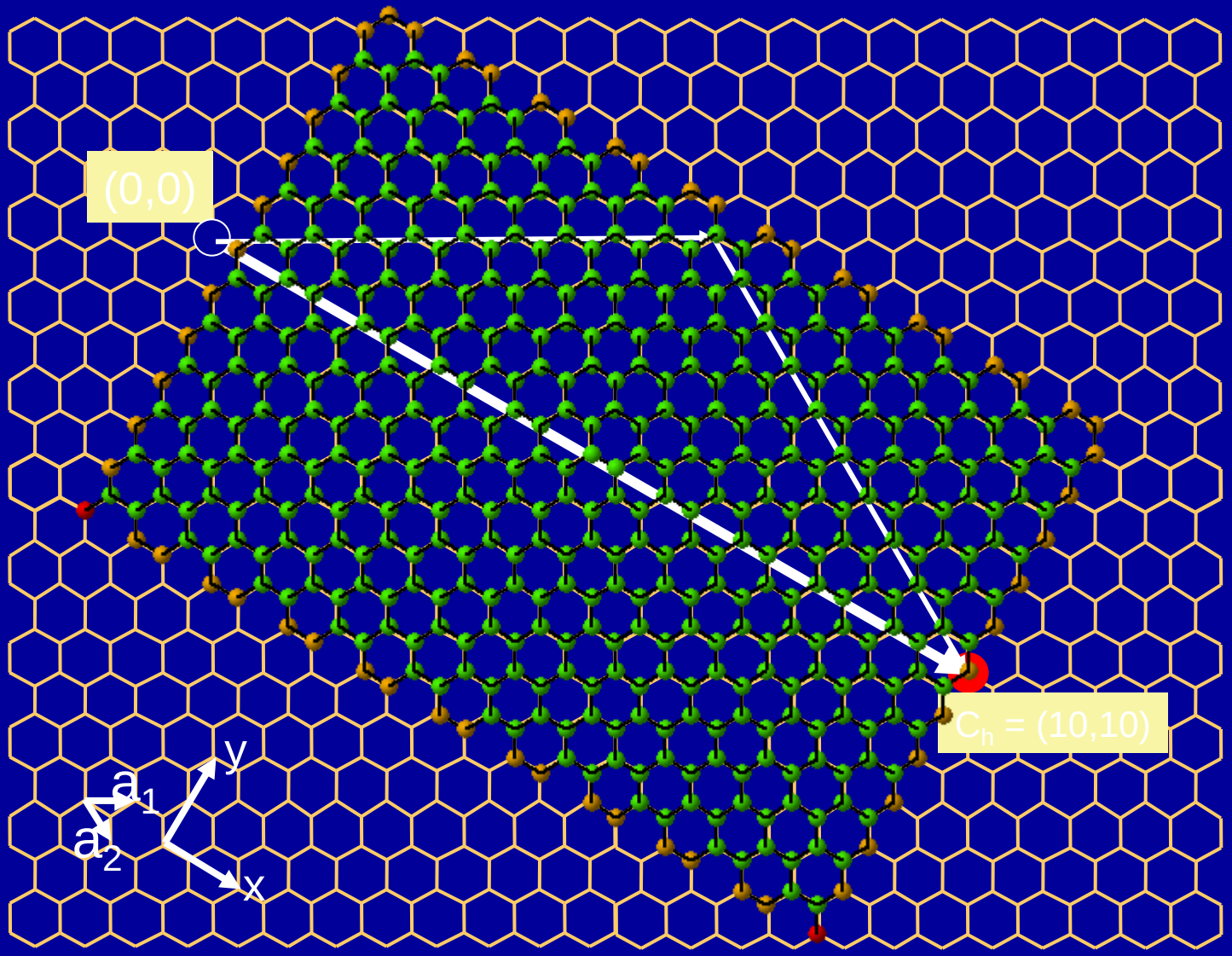

Wrapping (10,5) SWNT (chiral)

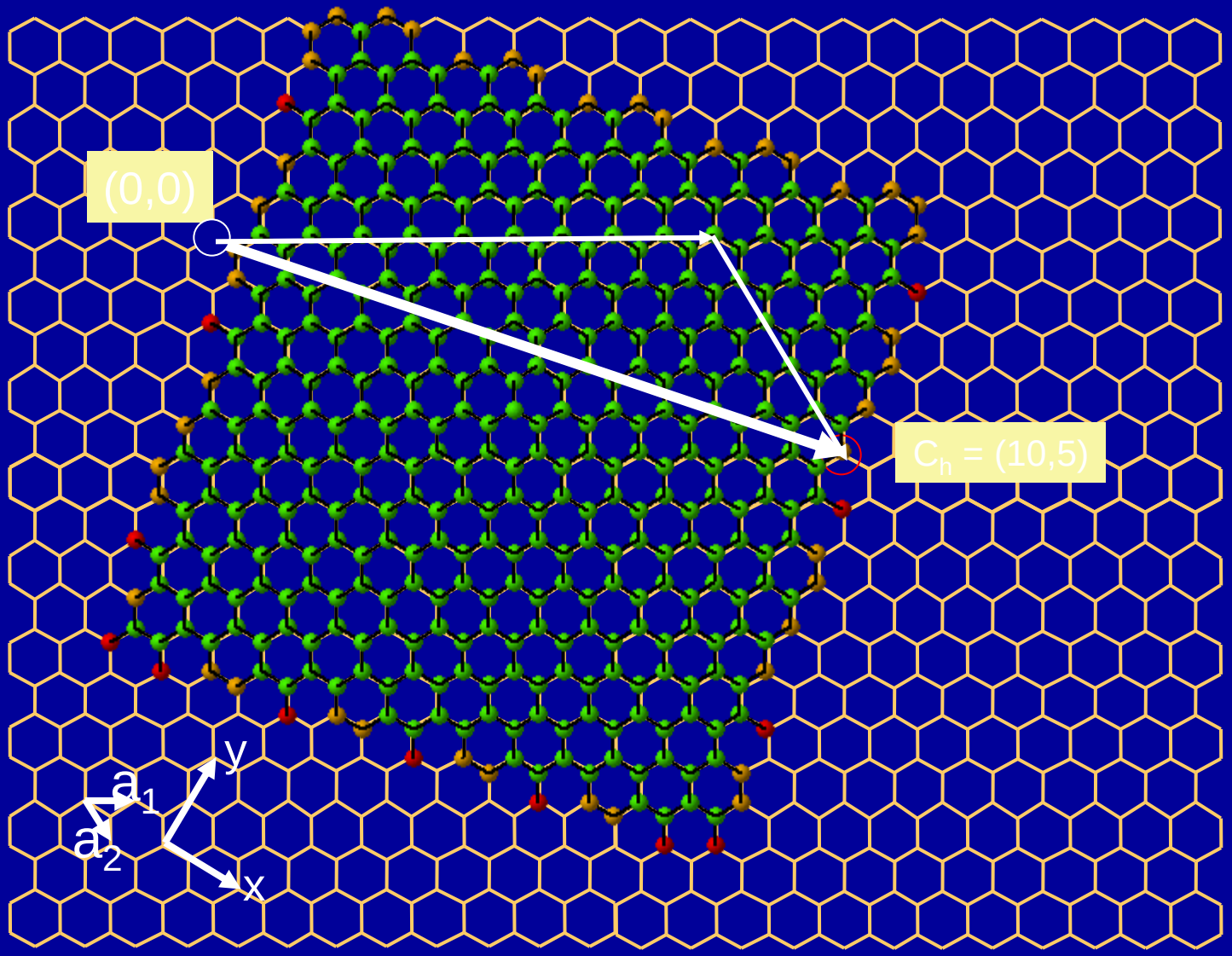

Wrapping (10,5) SWNT

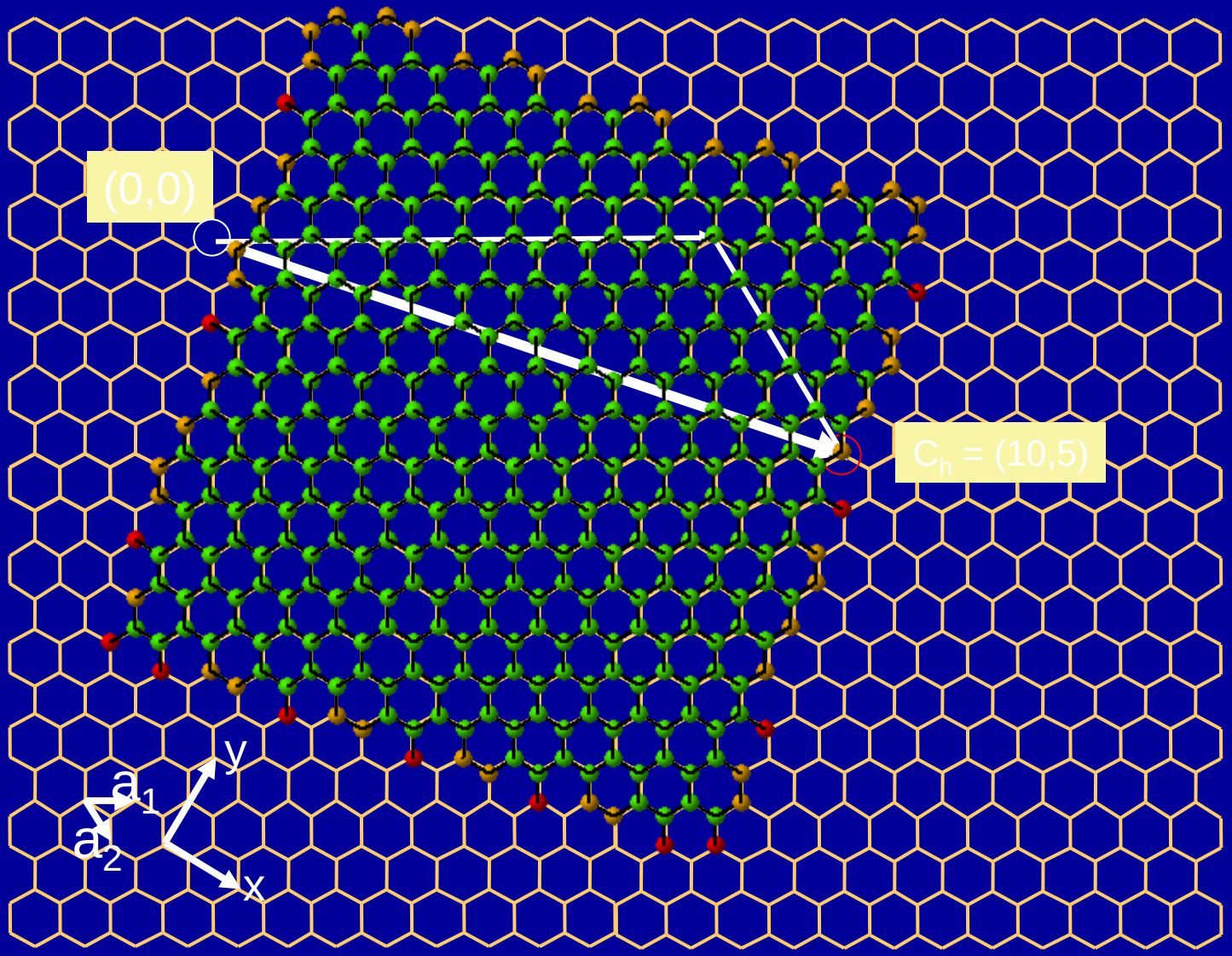

Hexagonal Lattice (n,m) nanotubes

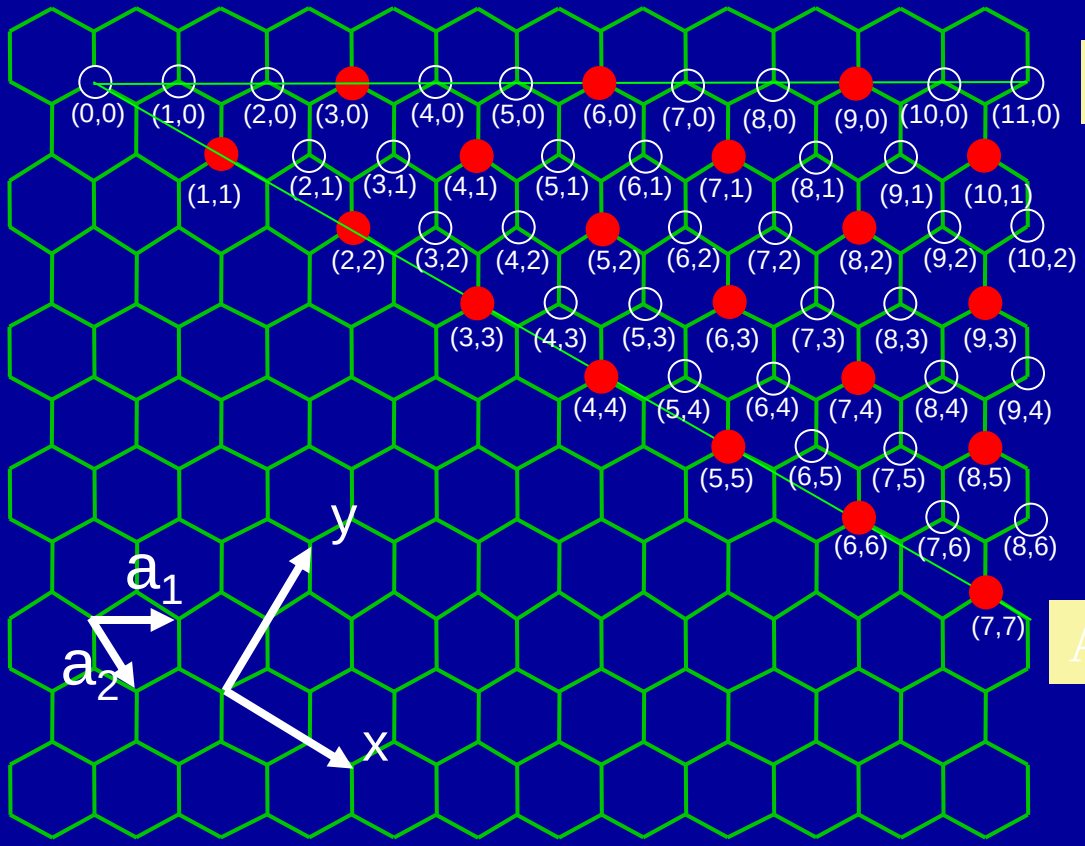

n - m = 3q (q: integer): metallic

n - m ≠ 3q (q: integer): semiconductor

Potential, Current and Ancient Applications

- The strength and flexibility of carbon nanotubes makes them of potential use in controlling other nanoscale structures, which suggests they will have an important role in nanotechnology engineering. The highest tensile strength an individual multi-walled carbon nanotube has been tested to be is 63 GPa. Bulk nanotube materials may never achieve a tensile strength similar to that of individual tubes, but such composites may nevertheless yield strengths sufficient for many applications. Carbon nanotubes have already been used as composite fibers in polymers and concrete to improve the mechanical, thermal and electrical properties of the bulk product. Carbon nanotubes have also recently been discovered to be a component of damascus steel, which accounts for why those ancient swords made from it were reported to have been able to cut through stone and metal without losing their edge, to the point where they could still cut silk scarves in mid-air.

Structural

- Because of the great mechanical properties of the carbon nanotubule, a variety of structures have been proposed ranging from everyday items like clothes and sports gear to combat jackets, space elevators and contraceptives. However the space elevator will require further efforts in refining carbon nanotube technology, as the practical tensile strength of carbon nanotubes can still be greatly improved..For perspective outstanding breakthroughs have already been born. Pioneering work lead by Ray H. Baughman at the NanoTech Institute has shown that single and multi-walled nanotubes can produce materials with toughness un-matched in the man-made and natural worlds.
- A good example of a practical use for the carbon nanotubules is the bicycle Floyd Landis used at the 2006 Tour de France. Carbon nanotubes were used to enhance the strength of the carbon fiber frame and made it possible to make a bicycle's frame weighing only one kilogram.

IN ELECTRICAL CIRCUITS

- Carbon nanotubes have many properties—from their unique dimensions to an unusual current conduction mechanism—that make them ideal components of electrical circuits. Currently, there is no reliable way to arrange carbon nanotubes into a circuit.The major hurdles that must be jumped for carbon nanotubes to find prominent places in circuits relate to fabrication difficulties. The production of electrical circuits with carbon nanotubes are very different from the traditional IC fabrication process. The IC fabrication process is somewhat like sculpture - films are deposited onto a wafer and pattern-etched away. Because carbon nanotubes are fundamentally different from films, carbon nanotube circuits can not be mass produced as of now.

Tiny tubes of carbon could oust plasma in large flat-panel displays

- NOW THAT PLASMA TELEVISIONS ARE HERE,
- their makers would have you believe the quest for the ultimate TV is
- over. After all, these big, flat screens are dazzlingly bright and have a
- wide viewing angle. They can be hung on a wall or even built right into
- it. What more could you want?
- Well, for starters, how about a TV set that doesn't consume as much power
- as a toaster oven? For that matter, youwould think that any TV technology worthy
- of the term "ultimate" would be free of significant flaws, which lower-end
- plasma screens are not. For example, many models costing less than about US
- $5000 have a distracting tendency to render pure black with a greenish cast.
- For reasons like those, bands of researchers in the United States, Europe,
- and Asia are insisting that the last word in TVs won't be plasma, but rather
- nanotubes. These exotic molecules of carbon, only a few nanometers wide and
- perhaps a micrometer long, are at the heart of a new class of big, bright experimental
- displays that could overcome the power and image quality problems
- of plasma screens while retaining their brightness and size.

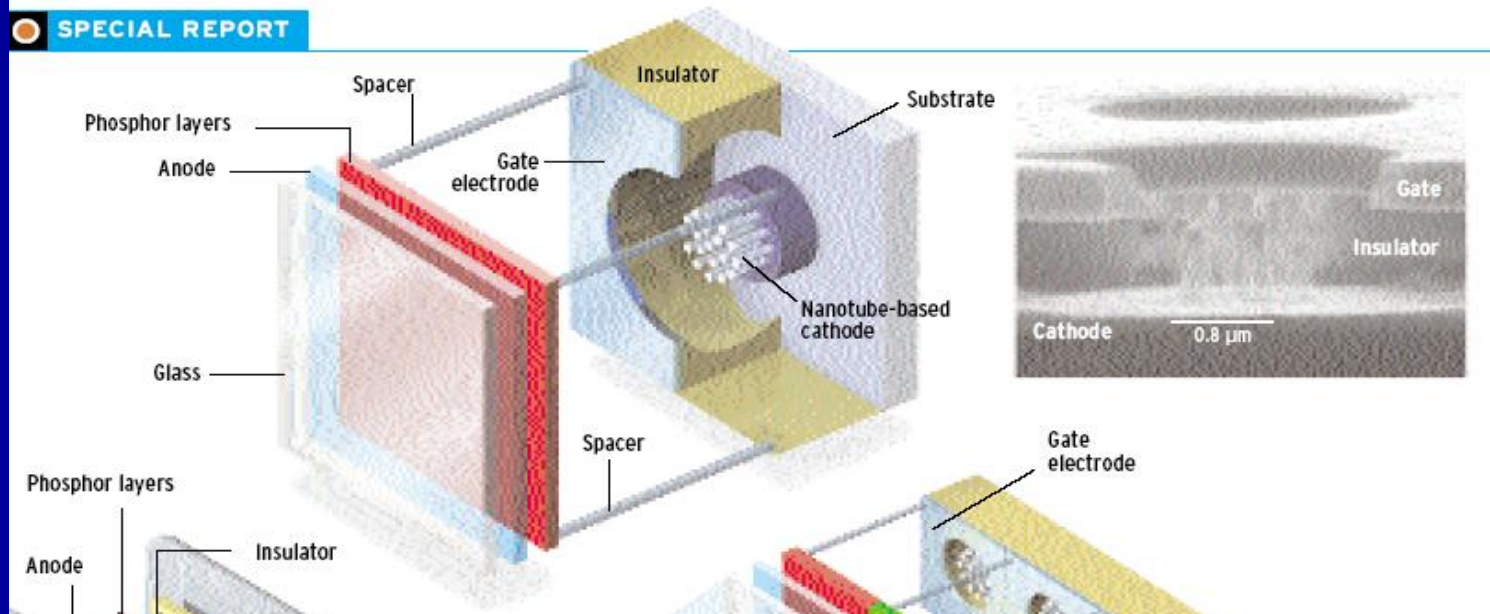

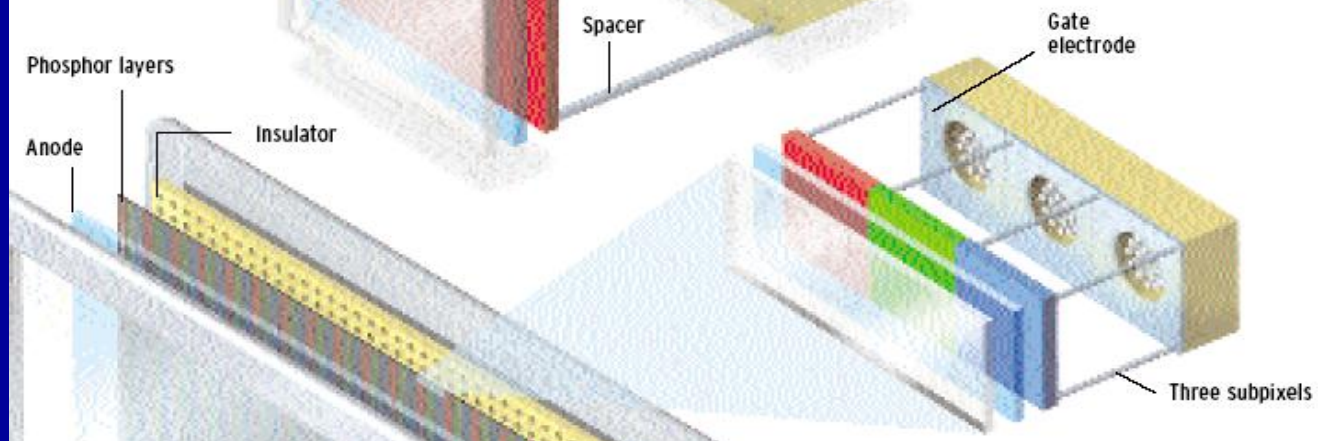

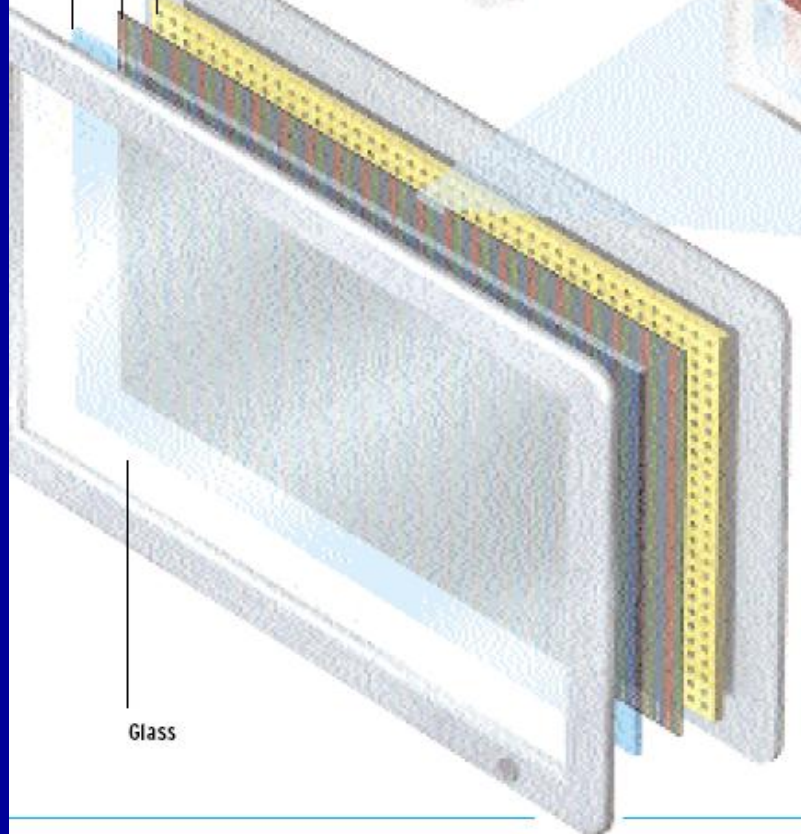

Thin Television

The heart of a field-emission display is an array of carbon nanotube-based emitters. In this design, a cluster of nanotubes at each emitter act as a cathode to produce electrons via field-emission [top left]. Each pixel is composed of three red, green, and blue sub-pixels [above], with their colors combined to create any color. A gate electrode in each sub-pixel creates the electric field for emission [also shown in photomicrograph, top]. Emitted electrons are swept through a vacuum toward a phosphor by an anode placed between the phosphor and the glass surface of the display [left]. Struck by the electrons, the phosphor emits visible light, as in a traditional cathode ray tube, but in a package that's a fraction the thickness [left].

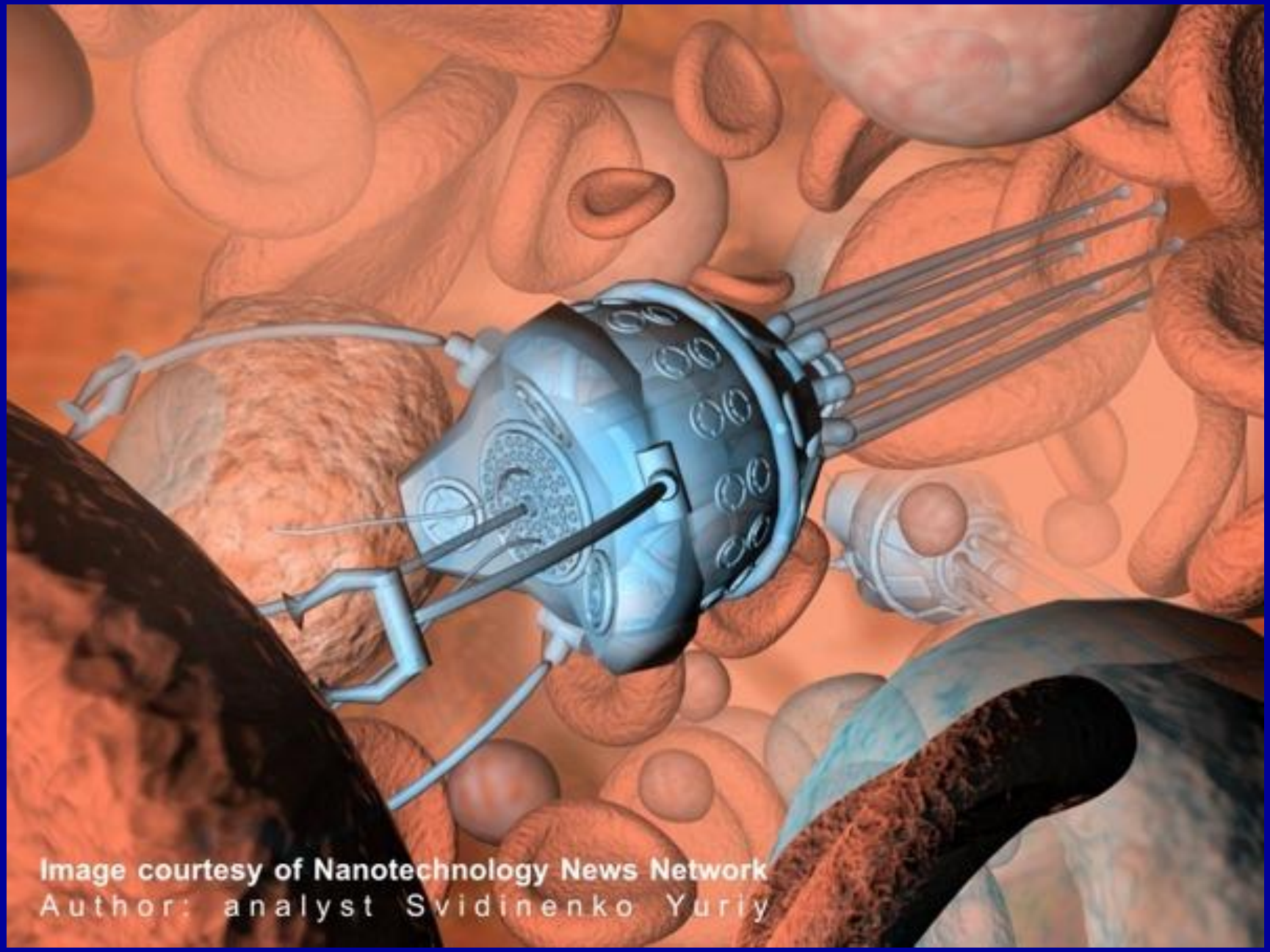
Image courtesy of Nanotechnology News Network
Author: analyst Svidinenko Yuriy

Golden nanotubes show super contrast Sep 10, 2009

- Researchers in Arkansas in the US have developed new nanomaterials – dubbed golden nanotubes – for use as super contrast agents for highly sensitive imaging of tumours and cancer cells. When intravenously injected with the nanotubes, mice with tumours in their lymph nodes show photoacoustic and photothermal signals that are 100 times stronger than those observed for ordinary carbon nanotubes. The nanomaterial, which can also be used to carry therapeutic agents thanks to its hollow core, could be used as a more efficient and less toxic alternative to other nanoparticles and fluorescent labels for non-invasive tumour imaging

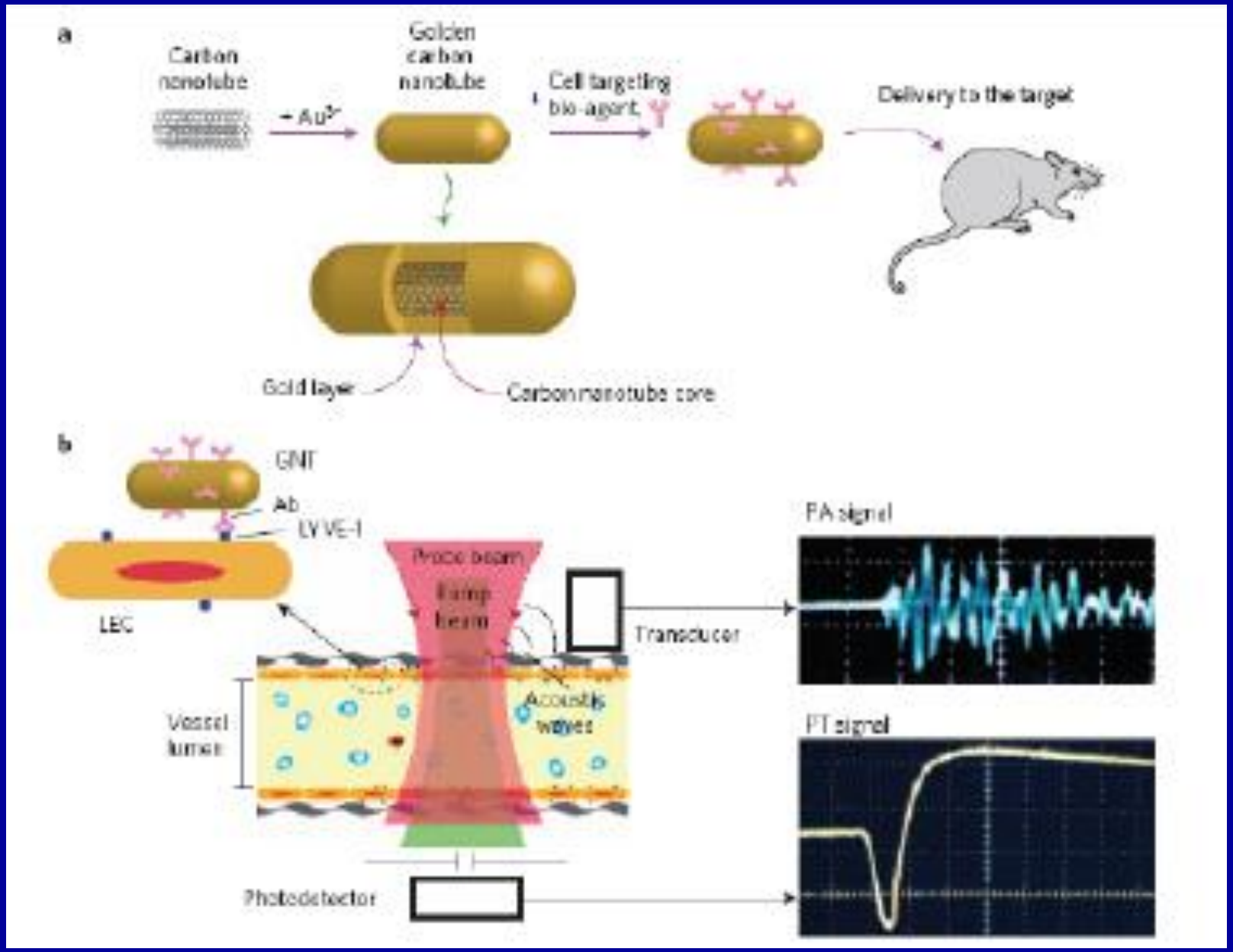
a
Carbon nanotube
Au3+
Golden carbon nanotube
Cell targeting bio-agent
Delivery to the target
Gold layer
Carbon nanotube core
b
GNT
Ab
LYVE-1
LEC
Probe beam
Pump beam
Transducer
Vessel lumen
Acoustic waves
Photodetector
PA signal
PT signal

Technology update
Sep 15, 2009

- **Nanotubes set to shine for solar energy**
- Carbon nanotubes could be used to produce solar cells that generate more electrical current per photon than existing photovoltaic technologies, according to scientists in the US. The team has shown that photodiodes made from carbon nanotubes create multiple electron-hole pairs in response to a single photon – unlike other photodiodes, which produce just one pair per photon.
- "If this could be exploited in large-scale solar cells, it would extend the power conversion efficiency above standard limits," said Nathan Gabor of Cornell University, who was involved in the research.

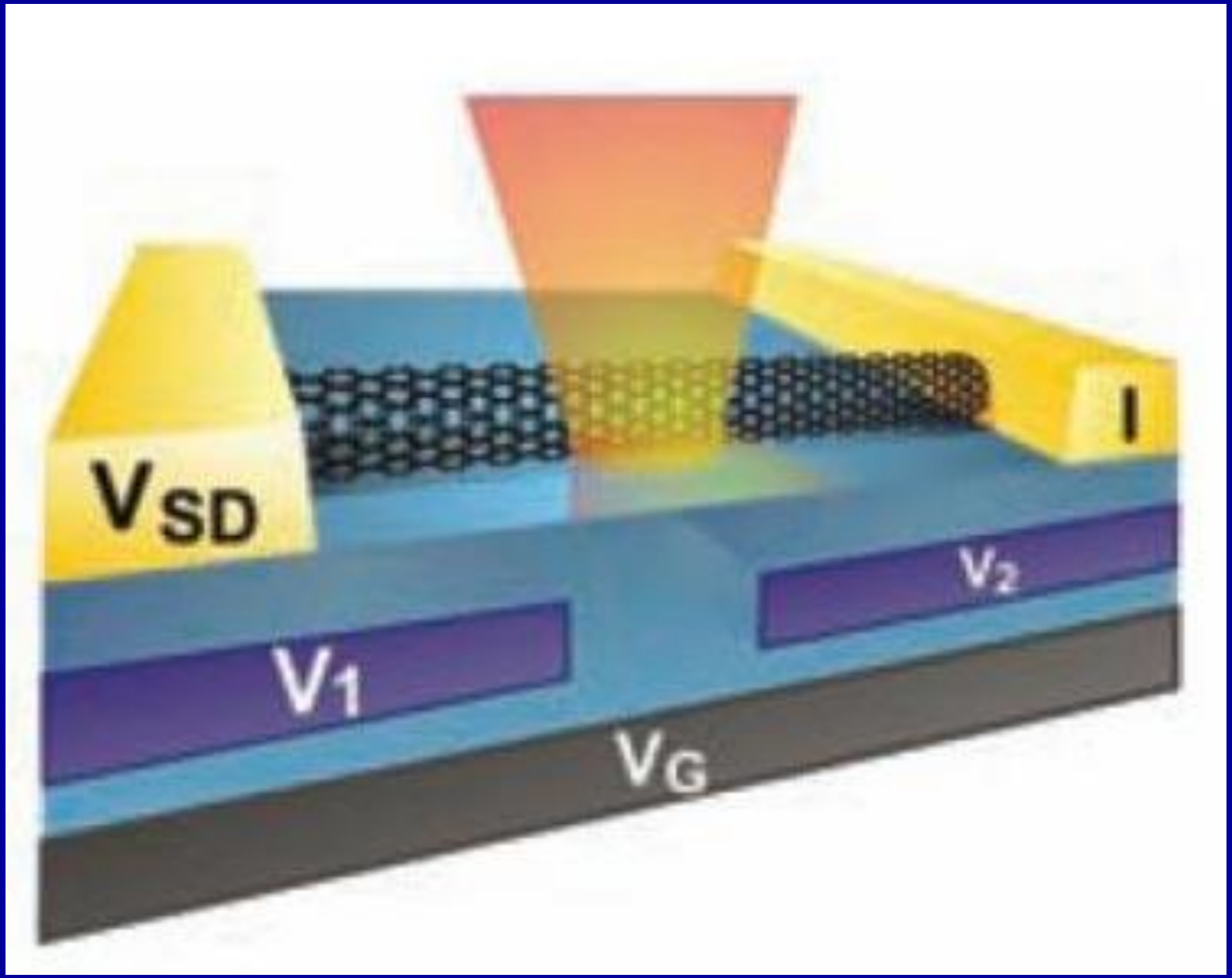
V_SD
I
V_2
V_1
V_G

PLAY MEDIA OF NANOTUBE

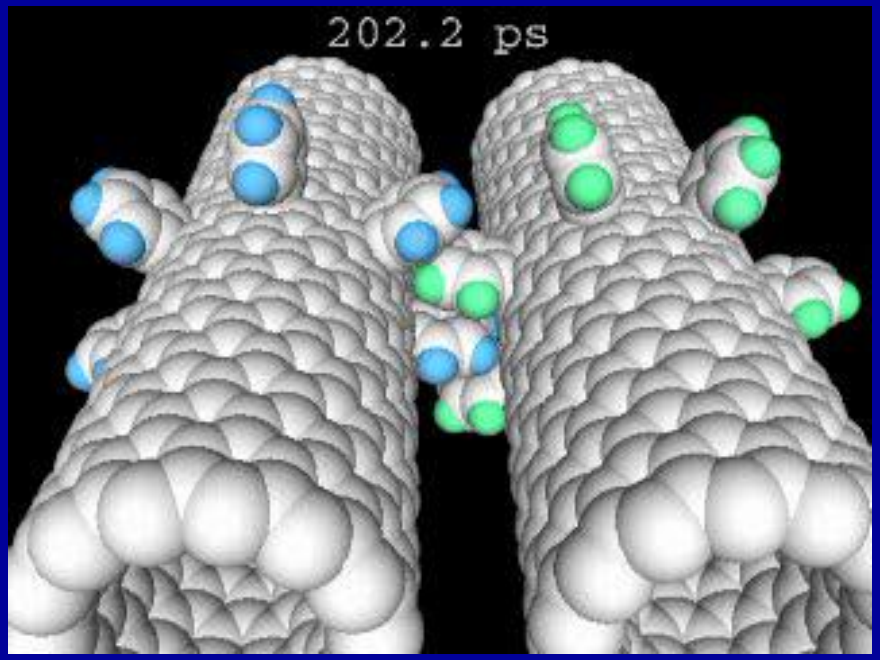

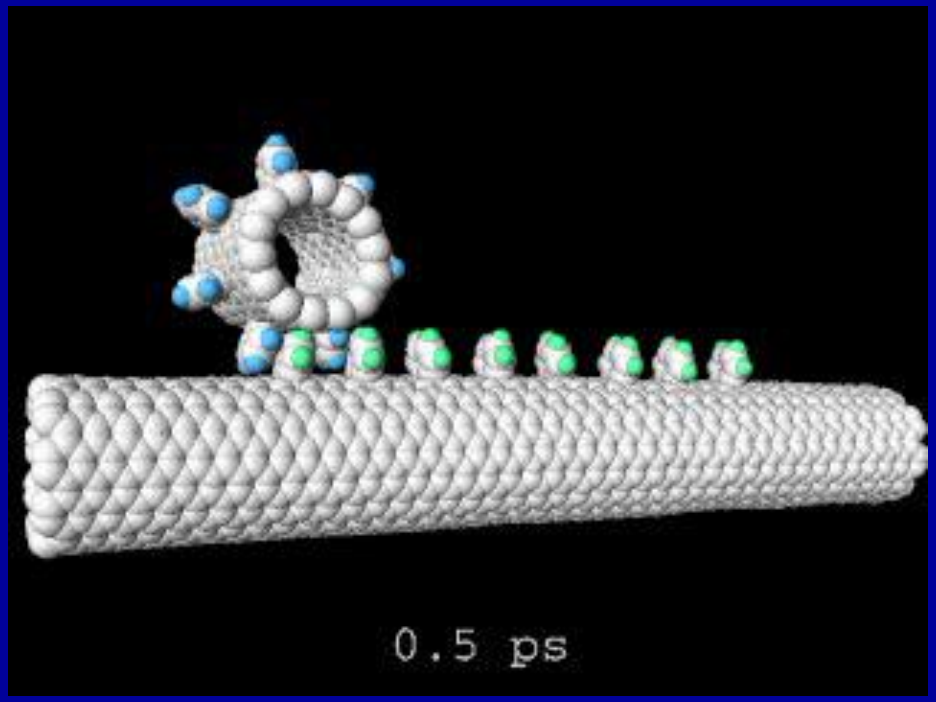

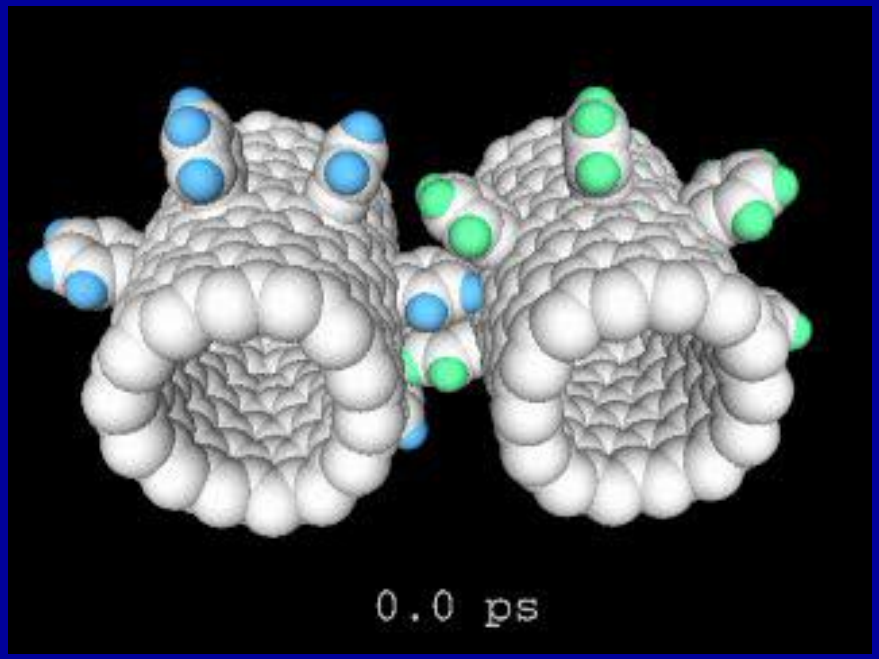
0.0 ps

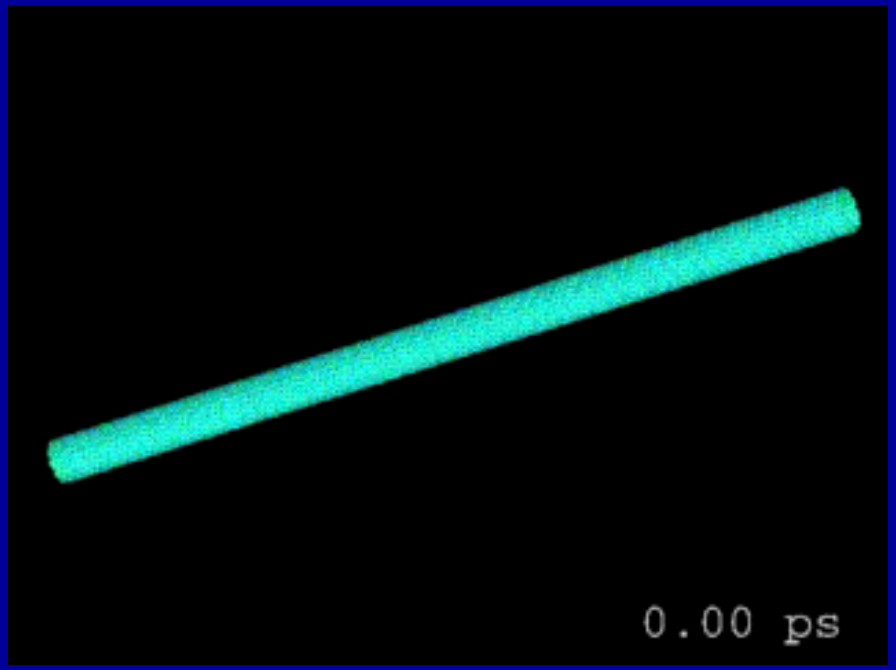
0.00 ps

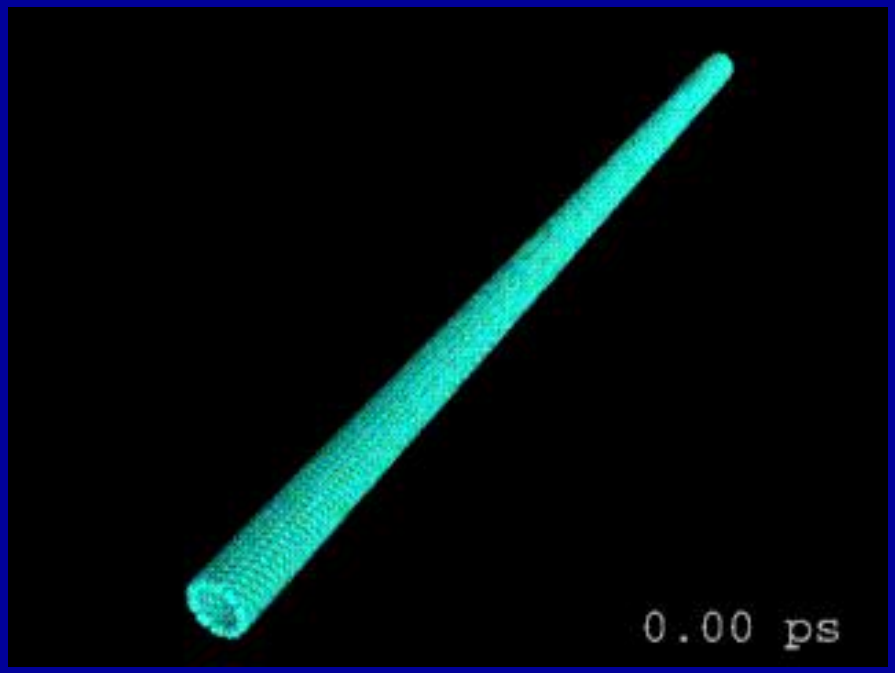
0.00 ps

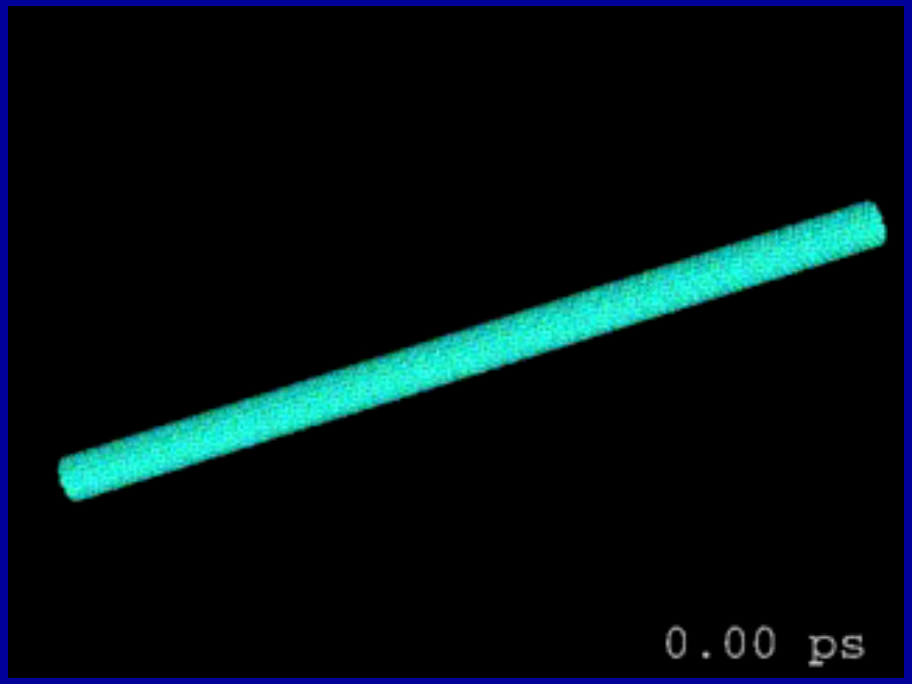
0.00 ps

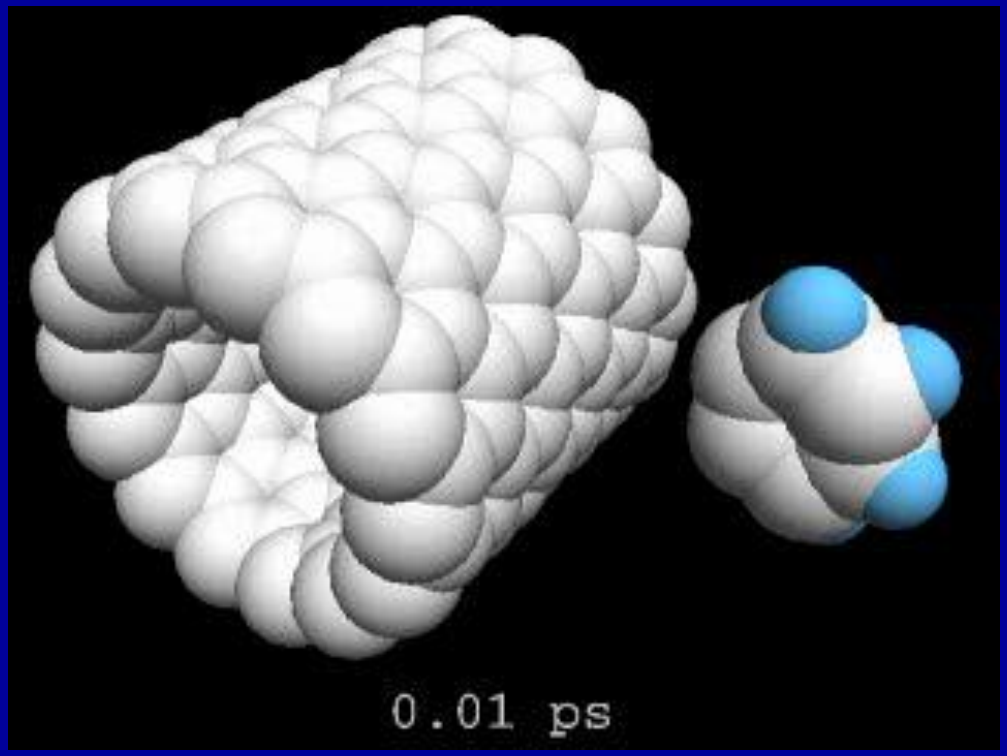
0.01 ps

Nanoshells

Nanoshells kill tumor cells selectively

Nanoscale Cantilevers

Cantilevers detect biomarkers of cancer

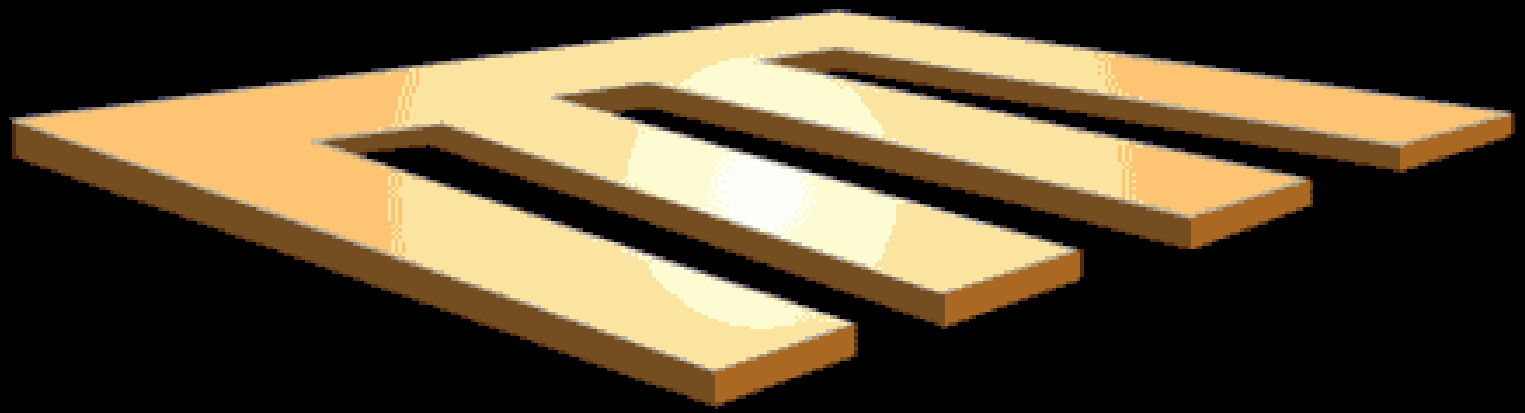

PUBLICATIONS IN THE AREA OF NANOTUBES

Mensah S.Y., Allotey F.K.A., Mensah N.G. and Nkrumah G. Differential Thermopower of a CNT Chiral Carbon Nanotube. *J. Phys. : Condens Matter 13* (2001) 5653-5662.

Mensah S.Y., Allotey F.K.A., Mensah N.G. and Nkrumah G. Giant Electrical Power Factor in Single-Walled Chiral Carbon Nanotube *Preprint of International Centre for Theoretical Physics* Trieste (2001)IC143 1-8.

Mensah S.Y., Allotey F.K.A., Mensah N.G. and Nkrumah G. Electronic Properties of Single-Walled Chiral Carbon Nanotube. *International Centre for Theoretical Physics* (2001) IC118 1 - 17.

S.Y. Mensah.,F.K.A. Allotey., George Nkrumah and N.G. Mensah High Electron Thermal Conductivity Of Chiral Carbon Nanotubes *International Centre for Theoretical Physics* (2003) IC1 46 1 - 13.

S.Y. Mensah., F.K.A. Allotey., N.G. Mensah., and G. Nkrumah. Giant Electrical Power Factor in Single-walled Chrial Carbon Nanotube. Superlattices and Microstructures 33 (2003) 173 – 180.

- S.Y. Mensah., F.K.A. Allotey., G. Nkrumah, and N.G. Mensah. High Electron Thermal Conductivity of Chiral Carbon Nanotubes. Physica E 23 (2004) 152 – 158.

- N.G. Mensah., G. Nkrumah., S.Y. Mensah., and F.K.A. Allotey. Temperature Dependence of the Thermal Conductivity in Chiral Carbon Nanotubes. Physica Letters A 329 (2004) 369 – 378.

THERMOELECTRIC FIGURE OF MERIT OF CHIRAL CARBON NANOTUBE

PRESENTED BY
PROF. S. Y. MENSAH

(DEAN : FACULTY OF SCIENCE)

Collaborators

DR. N.

G. Mensah, G. K. Nkrumah-Buandoh, PROF. F. K. A. Allotey and A. Twum

MOTIVATION

Thermoelectric Effect and Applications

- **Seebeck effect**

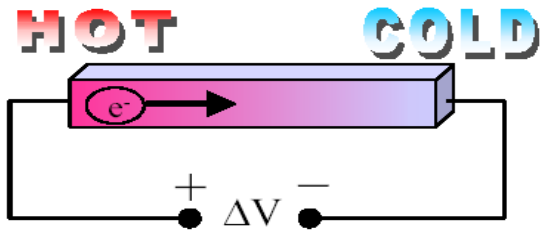

$$S = -\frac{\Delta V}{\Delta T}$$

$S > 0$ for p-type
$S < 0$ for n-type

- **Thermoelectric cooling**
  - No moving parts
  - Can be integrated with electronic circuits (e.g. CPU)
  - Environmentally friendly
  - Localized cooling with rapid response

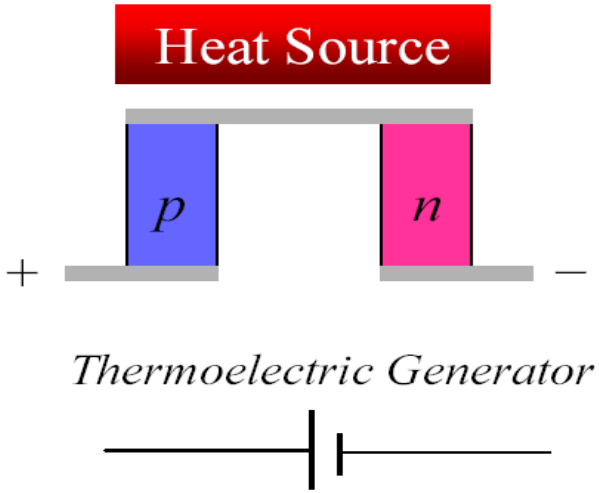

- **Power Generation**
  - Use waste heat to generate electricity

Application of Low Dimensionality for enhancing thermoelectric Performance

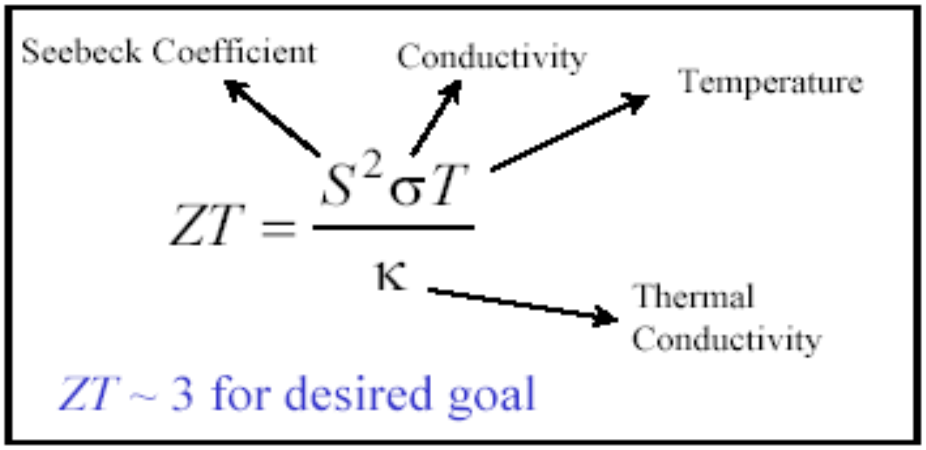

Difficulties in increasing ZT in bulk materials:

$S \uparrow \Longleftrightarrow \sigma \downarrow$

$\sigma \uparrow \Longleftrightarrow S \downarrow$ and $\kappa \uparrow$

$\Rightarrow$ A limit to Z is rapidly obtained in conventional materials

$\Rightarrow$ So far, best bulk material ($Bi_{0.5}Sb_{1.5}Te_3$) has $ZT \sim 1$ at 300 K

Low dimensions give additional control:

- Enhanced density of states due to quantum confinement effects
  $\Rightarrow$ Increase S without reducing σ
- Boundary scattering at interfaces reduces κ more than σ
- Possibility of carrier pocket engineering to get thermoelectric contribution in both quantum well and barrier regions

Thermoelectric figure of merit of superlattices

J. O. Sofo and G. D. Mahan
Solid State Division, Oak Ridge National Laboratory, P.O. Box 2008, Oak Ridge, Tennessee 37831-6030, and Department of Physics and Astronomy, The University of Tennessee, Knoxville, Tennessee 37996-1200

(Received 13 June 1994; accepted for publication 19 September 1994)

We calculate the electrical conductivity, thermopower, and the electronic contribution to the thermal conductivity of a superlattice, with the electric field and the thermal gradient applied parallel to the interfaces. We include the tunneling between quantum wells. The broadening of the lowest subband when the period of the superlattice is decreased produces a reduction of the thermoelectric figure of merit. However, we found that a moderate increase of the figure of merit may be expected for intermediate values of the period, due to the enhancement of the density of states produced by the superlattice structure. © *1994 American Institute of Physics.*

During the last two years, several papers were published analyzing the application of quantum well superlattices to improve the efficiency of thermoelectric coolers.[1–4] Experimental work is being done seeking the confirmation of the theoretical predictions.[5,6] To our knowledge, the first proposal that a superlattice structure may be a highly efficient thermoelement was done by Mensah and Kangah.[1] However, calculation of the transport properties of superlattices have been previously reported.[7–9] The first quantitative result was given by Hicks,[2] where a huge increase of the thermoelectric figure of merit is predicted as the width of the quantum wells is reduced. The thermoelectric figure of merit is a measure of the quality of a material to be used as a thermoelement[10] and is defined as $Z=S^2\sigma/\kappa$, where S is the thermopower, σ the electrical conductivity, and κ the thermal conductivity. Z has units of inverse temperature and is usually referred to as the dimensionless quantity ZT, where T is the absolute temperature. Hicks' calculation was welcome by both the workers on thermoelectric devices and those in the field of semiconductors superlattices. The former are seeking for creative ideas

action, the problem is reduced to the study of electrons with effective mass components m_x, m_y, and m_z in a potential profile with rectangular barriers as in the Kronig–Penney model.[12] The energy levels in the superlattice are given by

$$\epsilon_s(k_x,k_y,k_z)=\frac{\hbar^2k_x^2}{2m_x}+\frac{\hbar^2k_y^2}{2m_y}+E_s(k_z), \tag{1}$$

where k_x and k_y are the wave vectors in the x and y direction (parallel to the plane of the interfaces) and $E_s(k_z)$ is the dispersion relation of the subband s of the superlattice. This dispersion relation is obtained as a solution of the Kronig–Penney model that can be found in many introductory books on electron states in crystals.[13]

We will calculate these coefficients in the simplest possible form in order to make more evident the effects produced by the superlattice structure. Assuming a constant relaxation time we can carry out that the integration over the momentum components parallel to the interfaces, obtaining that

theoretical predictions.[5,6] To our knowledge, the first proposal that a superlattice structure may be a highly efficient thermoelement was done by Mensah and Kangah.[1] However, calculation of the transport properties of superlattices have been previously reported.[7–9] The first quantitative result was given by Hicks,[2] where a huge increase of the thermoelectric

[1] S. Y. Mensah and G. K. Kangah, J. Phys.: Condens. Matter **4**, 919 (1992).
[2] L. D. Hicks and M. D. Dresselhaus, Phys. Rev. B **47**, 12 727 (1993).

MOTIVATION CONT'D

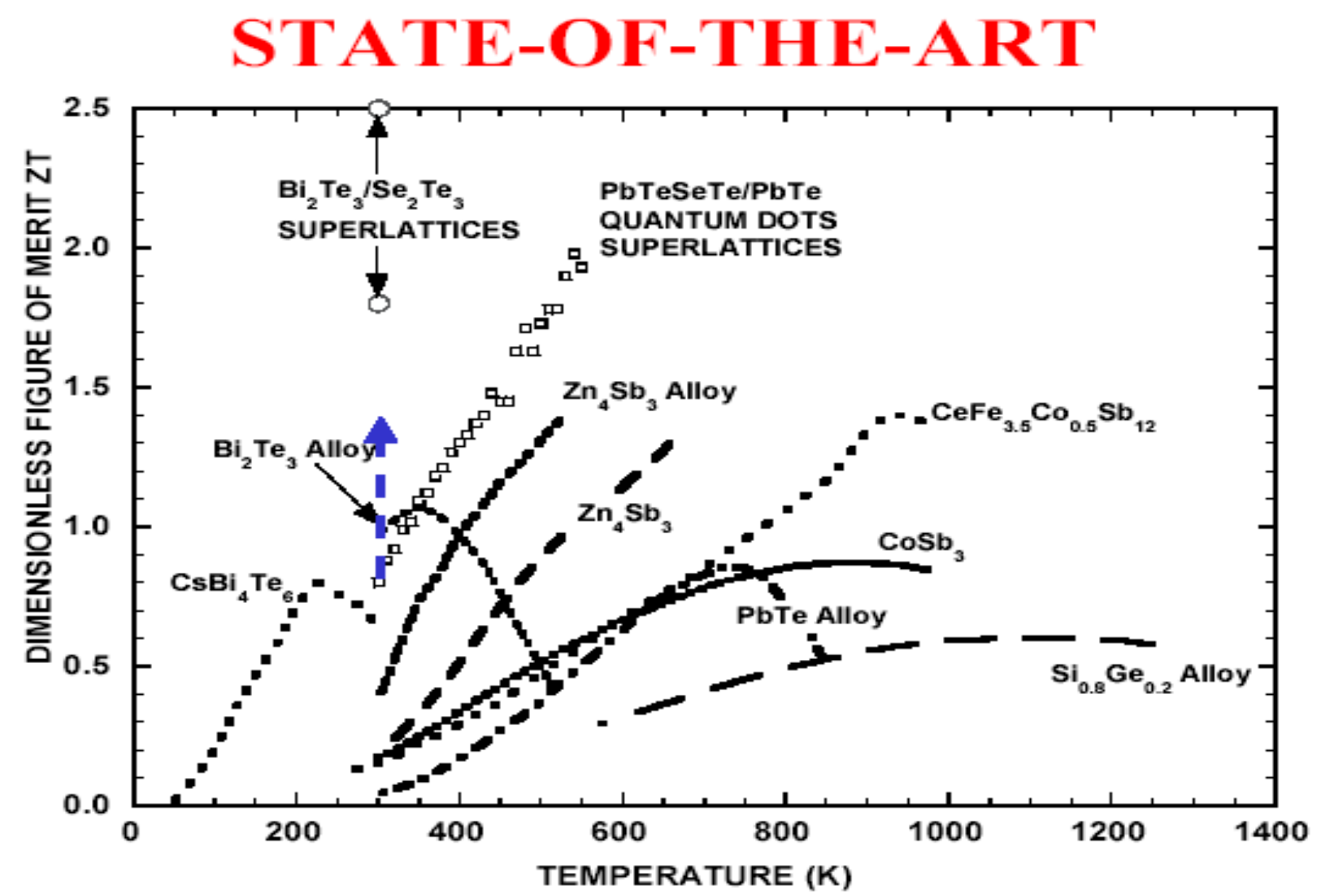

THEORY

We calculate the electron conductivity, the Peltier coefficient (and hence the thermopower), the zero-current density electron thermal conductivity and the figure of merit of CNT.We use the approach developed in[16, 17, 20, 21]. We noted that the properties mentioned above strongly depend on the GCA θh, temperature T and real overlapping integrals for jumps along the tubular axis Δz and the base helix Δs. The variation of these parameters can give rise to giant thermopower, unusual high electron thermal conductivity and the figure of merit greater than 1, making CNT very good material for the production of thermoelement.

Single walled-carbon nanotube (SWNT) is considered as an infinitely long chain of carbon atoms wrapped along a base helix. The problem is considered in the semiclassical approximation, starting with the Boltzmann kinetic equation[13],

$$\frac{\partial f(r,p,t)}{\partial t} + v(p)\frac{\partial f(r,p,t)}{\partial r} + eE\frac{\partial f(r,p,t)}{\partial p} = -\frac{f(r,p,t) - f_0(p)}{\tau} \qquad (1)$$

Here *f(r, p, t)* is the distribution function, *f0(p)* is the equilibrium distribution function, *v(p)* is the electron velocity, E is a weak constant applied field, *r* is the electron position, *p* is the electron dynamical momentum, τ is the relaxation time and *e* is the electron charge.

THEORY

The collision integral is taken in the *τ* approximation and further assumed constant. Eq.(1) is solved by perturbation approach treating the second term as the perturbation. In the linear approximation of T and μ, μ is the chemical potential, we obtain

$$f(p) = \tau^{-1}\int_0^{\infty}\exp\left(-\frac{t}{\tau}\right)f_0(p-eEt)dt + \int_0^{\infty}\exp\left(-\frac{t}{\tau}\right)dt \times\left(\left[\varepsilon(p-eEt)-\mu\right]\frac{\nabla T}{T}+\nabla\mu\right)v(p-eEt)\frac{\partial f_0(p-eEt)}{\partial\varepsilon} \qquad (2)$$

here *ε(p)* is the electron energy. The current density **j** is defined as

$$\mathbf{j} = e\sum_p \mathbf{v}(p)f(p) \qquad (3)$$

and the thermal current density **q** as

$$\mathbf{q} = \sum_p \left[\varepsilon(p)-\mu\right]\mathbf{v}(p)f(p) \qquad (4)$$

Substituting Eq. (2) into Eqs. (3) and (4), and making the transformation

$p - eEt \rightarrow p$

we obtain for the current density

$$\begin{aligned}
\mathbf{j} \;=\; & e\tau^{-1}\int_0^\infty \exp\left(-\frac{t}{\tau}\right) dt \sum_p \mathbf{v}(p-eEt) f_0(p) + \\
& + e\int_0^\infty \exp\left(-\frac{t}{\tau}\right) dt \sum_p \left([\varepsilon(p)-\mu]\frac{\nabla T}{T} + \nabla\mu \right) \times \\
& \times \left(\mathbf{v}(p)\frac{\partial f_0(p)}{\partial \varepsilon} \right) \cdot \mathbf{v}(p-eEt) \qquad (5)
\end{aligned}$$

and for the thermal current density

$$\begin{aligned}
\mathbf{q} \;=\; & \tau^{-1}\int_0^\infty \exp\left(-\frac{t}{\tau}\right) dt \sum_p \left[\varepsilon\left(p-eEt\right)-\mu\right] \mathbf{v}(p-eEt) f_o\left(p\right) + \\
& + \int_0^\infty \exp\left(-\frac{t}{\tau}\right) dt \sum_p \left[\varepsilon\left(p-eEt\right)-\mu\right] \left\{ \left[\varepsilon\left(p\right)-\mu\right]\frac{\nabla T}{T} + \nabla\mu \right\} \times \\
& \times \left\{ v\left(p\right)\frac{\partial f_o\left(p\right)}{\partial \varepsilon} \right\} \mathbf{v}(p-eEt) \qquad (6)
\end{aligned}$$

We resolve Eqs. (5) and (6) along the tubular axis (z axis) and the base helix, neglecting the interference between the axial and the helical paths connecting a pair of atoms, so that transverse motion quantizatoin is ignored24, 25, 26. This approximation best describes doped chiral carbon nanotubes, and is experimentally confirmed in27. Using the following transformation

$$\sum_{p} \rightarrow \frac{2}{(2\pi\hbar)^2} \int_{-\frac{\pi}{d_s}}^{\frac{\pi}{d_s}} dp_s \int_{-\frac{\pi}{d_z}}^{\frac{\pi}{d_z}} dp_z$$

we obtain the electron current density along the tubular axis and the base helix as

$$\begin{aligned} Z'_j &= \frac{2e\tau^{-1}}{(2\pi\hbar)^2} \int_0^{\infty} \exp\left(-\frac{t}{\tau}\right) dt \int_{-\pi/d_s}^{\pi/d_s} dp_s \int_{-\pi/d_z}^{\pi/d_z} dp_z v_z(p - eEt) f_0(p) + \\ &+ \frac{2e}{(2\pi\hbar)^2} \int_0^{\infty} \exp\left(-\frac{t}{\tau}\right) dt \int_{-\pi/d_s}^{\pi/d_s} dp_s \int_{-\pi/d_z}^{\pi/d_z} dp_z \\ &\times \left\{ [\varepsilon(p) - \mu] \frac{\nabla_z T}{T} + \nabla_z \mu \right\} \left\{ v_z(p) \frac{\partial f_0(p)}{\partial \varepsilon} \right\} v_z(p - eEt) \end{aligned} \quad (7)$$

and

$$
\begin{aligned}
S'_j &= \frac{2e\tau^{-1}}{(2\pi\hbar)^2}\int_0^{\infty}\exp\left(-\frac{t}{\tau}\right)dt\int_{-\pi/d_s}^{\pi/d_s}dp_s\int_{-\pi/d_z}^{\pi/d_z}dp_z v_s(p-eEt)f_0(p)\\
&+\frac{2e}{(2\pi\hbar)^2}\int_0^{\infty}\exp\left(-\frac{t}{\tau}\right)dt\int_{-\pi/d_s}^{\pi/d_s}dp_s\int_{-\pi/d_z}^{\pi/d_z}dp_z\\
&\times\left\{\left[\varepsilon(p)-\mu\right]\frac{\nabla_s T}{T}+\nabla_s\mu\right\}\left\{v_s(p)\frac{\partial f_0(p)}{\partial\varepsilon}\right\}v_s(p-eEt) \qquad (8)
\end{aligned}
$$

Similarly the thermal current density along the tubular and the base helix base become

$$
\begin{aligned}
Z'_q &= \frac{2\tau^{-1}}{(2\pi\hbar)^2}\int_0^{\infty}\exp\left(-\frac{t}{\tau}\right)dt\int_{-\frac{\pi}{d_s}}^{\frac{\pi}{d_s}}dp_s\int_{-\frac{\pi}{d_z}}^{\frac{\pi}{d_z}}dp_z\left[\varepsilon(p-eEt)-\mu\right]v_z(p-eEt)f_o(p)+\\
&+\frac{2}{(2\pi\hbar)^2}\int_0^{\infty}\exp\left(-\frac{t}{\tau}\right)dt\int_{-\frac{\pi}{d_s}}^{\frac{\pi}{d_s}}dp_s\int_{-\frac{\pi}{d_z}}^{\frac{\pi}{d_z}}dp_z\left[\varepsilon(p-eEt)-\mu\right]\times\\
&\times\left\{\left[\varepsilon(p)-\mu\right]\frac{\nabla_z T}{T}+\nabla_z\mu\right\}\left\{v_z(p)\frac{\partial f_o(p)}{\partial\varepsilon}\right\}v_z(p-eEt) \qquad (9)
\end{aligned}
$$

and

$$
\begin{aligned}
S'_q &= \frac{2\tau^{-1}}{(2\pi\hbar)^2}\int_0^{\infty}\exp\left(-\frac{t}{\tau}\right)dt\int_{-\frac{\pi}{d_s}}^{\frac{\pi}{d_s}}dp_s\int_{-\frac{\pi}{d_z}}^{\frac{\pi}{d_z}}dp_z\left[\varepsilon(p-eEt)-\mu\right]v_s(p-eEt)f_o(p)+\\
&+\frac{2}{(2\pi\hbar)^2}\int_0^{\infty}\exp\left(-\frac{t}{\tau}\right)dt\int_{-\frac{\pi}{d_s}}^{\frac{\pi}{d_s}}dp_s\int_{-\frac{\pi}{d_z}}^{\frac{\pi}{d_z}}dp_z\left[\varepsilon(p-eEt)-\mu\right]\times\\
&\times\left\{\left[\varepsilon(p)-\mu\right]\frac{\nabla_s T}{T}+\nabla_s\mu\right\}\left\{v_s(p)\frac{\partial f_o(p)}{\partial\varepsilon}\right\}v_s(p-eEt) \qquad (10)
\end{aligned}
$$

The integrations are carried out over the first Brillouin zone. The axial and circumferential electron current density will be given as follows

$$j_z = Z'_j + S'_j \sin\theta_h; \quad j_c = S'_j \cos\theta_h \tag{11}$$

and the axial and circumferential thermal current density also as

$$q_z = Z'_q + S'_q \sin\theta_h; \quad q_c = S'_q \cos\theta_h \tag{12}$$

where θ_h is the geometric chiral angle (GCA).

The energy *ε(p)* of the electrons, calculated using the tight binding approximation is givenas expressed in[25] as follows:

$$\varepsilon(p) = \varepsilon_o - \Delta_s \cos\frac{p_s d_s}{\hbar} - \Delta_z \cos\frac{p_z d_z}{\hbar} \tag{13}$$

εo is the energy of an outer-shell electron in an isolated carbon atom, Δs and Δz are the real overlapping integrals for jumps along the respective coordinates, *ps* and *pz* are the carrier momentum along the base helix and the tubular axis respectively, ħ is h/2π and h is Planck's constant. *ds* is the distance between the site *n* and *n + 1* along the base helix and *dz* is the distance between the site n and *n + N* along the tubular axis.

For a non-degenerate electron gas, we use the Boltzmann equilibrium distribution function f0(p) as expressed in [16], i.e.,

$$f_0(p) = C \exp\left(\frac{\Delta_s \cos\frac{p_s d_s}{\hbar} + \Delta_z \cos\frac{p_z d_z}{\hbar} + \mu - \varepsilon_o}{kT}\right) \qquad (14)$$

where C is determined by the condition

$$C = \frac{d_s d_z n_o}{2 \exp\left(\frac{\mu - \varepsilon_o}{kT}\right) I_0(\Delta_s^*) I_0(\Delta_z^*)}$$

and no is charge density, *In(x)* is the modified Bessel function of order *n* and *k* is Boltzmann's constant. The components v_s and v_z of the electron velocity v are given by

$$v_s(p_s) = \frac{\partial \varepsilon(p)}{\partial p_s} = \frac{\Delta_s d_s}{\hbar} \sin\frac{p_s d_s}{\hbar} \qquad (15)$$

and

$$v_z(p_z) = \frac{\partial \varepsilon(p)}{\partial p_z} = \frac{\Delta_z d_z}{\hbar} \sin\frac{p_z d_z}{\hbar} \qquad (16)$$

Using Eqs. (7)−(16) and the fact that $E_s = E_z \sin\theta_h$,

$\nabla T_s = T \sin\theta_h$, and $E = -\nabla\phi$, we obtain the following expressions

$$j_z = (\sigma_z + \sigma_s \sin^2\theta_h)\nabla_z\left(\frac{\mu}{e} - \phi\right) + \\ -\left\{\sigma_z \frac{k}{e}(\xi - \Delta_z^* B_z - \Delta_s^* A_s) + \right. \\ \left. + \sigma_s \frac{k}{e}\sin^2\theta_h (\xi - \Delta_s^* B_s - \Delta_z^* A_z)\right\}\nabla_z T \qquad (17)$$

$$j_c = \sigma_s \sin\theta_h \cos\theta_h \nabla_z\left(\frac{\mu}{e} - \phi\right) + \\ -\sigma_s \frac{k}{e}\sin\theta_h \cos\theta_h (\xi - \Delta_s^* B_s - \Delta_z^* A_z)\nabla_z T \qquad (18)$$

$$q_z = \frac{kT}{e}\{\sigma_z[\xi - \Delta_z^* B_z - \Delta_s^* A_s] + \sigma_s \sin^2\theta_h (\xi - \Delta_s^* B_s - \Delta_z^* A_z)\}\nabla_z\left(\frac{\mu}{e} - \phi\right) + \\ -\frac{k^2 T}{e^2}\left\{\sigma_z\left[\xi^2 - 2\Delta_z^*\xi B_z - 2\Delta_s^*\xi A_s + (\Delta_z^*)^2 C_z + \right.\right. \\ \left. + 2\Delta_z^*\Delta_s^* B_z A_s + (\Delta_s^*)^2\left(1 - \frac{A_s}{\Delta_s^*}\right)\right] + \sigma_s \sin^2\theta_h\left[\xi^2 - 2\Delta_s^*\xi B_s + \right. \\ \left.\left. -2\Delta_z^*\xi A_z + (\Delta_s^*)^2 C_s + 2\Delta_s^*\Delta_z^* B_s A_z + (\Delta_z^*)^2\left(1 - \frac{A_z}{\Delta_z^*}\right)\right]\right\}\nabla_z T \qquad (19)$$

Here

$$
\begin{aligned}
q_c &= \sigma_s \frac{kT}{e} \sin\theta_h \cos\theta_h \{\xi - \Delta_s^* B_s - \Delta_z^* A_z\} \nabla_z \left(\frac{\mu}{e} - \phi\right) + \\
&\quad -\sigma_s \frac{k^2 T}{e^2} \sin\theta_h \cos\theta_h \Big\{ \xi^2 - 2\Delta_s^* \xi B_s - 2\Delta_z^* \xi A_z + (\Delta_s^*)^2 C_s + \\
&\quad +2\Delta_s^* \Delta_z^* B_s A_z + (\Delta_z^*)^2 \left(1 - \frac{A_z}{\Delta_z^*}\right) \Big\} \nabla_z T \qquad (20)
\end{aligned}
$$

The thermal currrent density **q** given by Eqs. (19) and (20) can be written in terms of current density **j** as

$$
\begin{aligned}
q_z &= \frac{k}{e} \left[\frac{\sigma_z}{\sigma_z + \sigma_s \sin^2\theta_h} (\xi - \Delta_z^* B_z - \Delta_s^* A_s) \right. \\
&\quad \left. + \frac{\sigma_s \sin^2\theta_h}{\sigma_z + \sigma_s \sin^2\theta_h} (\xi - \Delta_s^* B_s - \Delta_z^* A_z) \right] T j_z \\
&\quad - \left[\frac{k^2 T}{e^2} \left(\sigma_z \Big\{ \xi^2 - 2\Delta_z^* \xi B_z - 2\Delta_s^* \xi A_s + (\Delta_z^*)^2 C_z + \right. \right. \\
&\quad \left. +2\Delta_z^* \Delta_s^* B_z A_s + (\Delta_s^*)^2 \left(1 - \frac{A_s}{\Delta_s^*}\right) \Big\} + \sigma_s \sin^2\theta_h \Big\{ \xi^2 - 2\Delta_s^* \xi B_s \right. \\
&\quad \left. \left. -2\Delta_z^* \xi A_z + (\Delta_s^*)^2 C_s + 2\Delta_s^* \Delta_z^* B_s A_z + (\Delta_z^*)^2 \left(1 - \frac{A_z}{\Delta_z^*}\right) \Big\} \right) \right. \\
&\quad \left. - (\sigma_z + \sigma_s \sin^2\theta_h) \frac{k^2 T}{e^2} \left(\frac{\sigma_z}{\sigma_z + \sigma_s \sin^2\theta_h} (\xi - \Delta_z^* B_z - \Delta_s^* A_s) + \right. \right. \\
&\quad \left. \left. + \frac{\sigma_s \sin^2\theta_h}{\sigma_z + \sigma_s \sin^2\theta_h} (\xi - \Delta_s^* B_s - \Delta_z^* A_z) \right)^2 \right] \nabla_z T \qquad (21)
\end{aligned}
$$

and

$$q_c = \frac{k}{e}(\xi - \Delta_s^* B_s - \Delta_z^* A_z) T j_c - \sigma_s \frac{k^2 T}{e^2} \sin\theta_h \cos\theta_h \left[\left\{ \xi^2 - 2\Delta_s^* \xi B_s - 2\Delta_z^* \xi A_z + \right.\right.$$
$$\left.\left. + (\Delta_s^*)^2 C_s + 2\Delta_s^* \Delta_z^* B_s A_z + (\Delta_z^*)^2 \left(1 - \frac{A_z}{\Delta_z^*}\right) \right\} - \{\xi - \Delta_s^* B_s - \Delta_z^* A_z\}^2 \right] \nabla_z T \qquad (22)$$

Hence from Eqs. (17) and (18) we obtain the axial and circumferential components of the electrical conductivity σ as follows

$$\sigma_{zz} = \sigma_z + \sigma_s \sin^2\theta_h \qquad (23)$$

$$\sigma_{cz} = \sigma_s \sin\theta_h \cos\theta_h \qquad (24)$$

From Eqs. (21) and (22) we also obtain the axial and circumferential components of Peltier coefficient Π, and the electron thermal conductivity χ_e when j is zero as follows

$$\Pi_{zz} = \alpha_{zz} T$$
$$= \frac{k}{e}\left[\frac{\sigma_z}{\sigma_z + \sigma_s \sin^2\theta_h} (\xi - \Delta_z^* B_z - \Delta_s^* A_s) \right.$$
$$\left. + \frac{\sigma_s \sin^2\theta_h}{\sigma_z + \sigma_s \sin^2\theta_h} (\xi - \Delta_s^* B_s - \Delta_z^* A_z) \right] T \qquad (25)$$

$$\Pi_{cz} = \alpha_{cz} T$$
$$= \frac{k}{e}(\xi - \Delta_s^* B_s - \Delta_z^* A_z) T \qquad (26)$$

where α is the thermopower or Seebeck coefficient.

$$\varkappa_{zz} = \frac{k^2T}{e^2}\Bigg(\sigma_z\Bigg\{\xi^2 - 2\Delta_z^*\xi B_z - 2\Delta_s^*\xi A_s + (\Delta_z^*)^2 C_z + $$
$$+2\Delta_z^*\Delta_s^* B_z A_s + (\Delta_s^*)^2\left(1 - \frac{A_s}{\Delta_s^*}\right)\Bigg\} + \sigma_s \sin^2\theta_h\Bigg\{\xi^2 - 2\Delta_s^*\xi B_s$$
$$-2\Delta_z^*\xi A_z + (\Delta_s^*)^2 C_s + 2\Delta_s^*\Delta_z^* B_s A_z + (\Delta_z^*)^2\left(1 - \frac{A_z}{\Delta_z^*}\right)\Bigg\}\Bigg)$$
$$-\frac{k^2T}{e^2}\left(\sigma_z + \sigma_s \sin^2\theta_h\right)\Bigg(\frac{\sigma_z}{\sigma_z + \sigma_s \sin^2\theta_h}\left(\xi - \Delta_z^* B_z - \Delta_s^* A_s\right) +$$
$$+\frac{\sigma_s \sin^2\theta_h}{\sigma_z + \sigma_s \sin^2\theta_h}\left(\xi - \Delta_s^* B_s - \Delta_z^* A_z\right)\Bigg)^2 \qquad (27)$$

$$\varkappa_{ez} = \sigma_s \frac{k^2T}{e^2}\sin\theta_h \cos\theta_h\Big[\Big\{\xi^2 - 2\Delta_s^*\xi B_s - 2\Delta_z^*\xi A_z +$$
$$+(\Delta_s^*)^2 C_s + 2\Delta_s^*\Delta_z^* B_s A_z + (\Delta_z^*)^2\left(1 - \frac{A_z}{\Delta_z^*}\right)\Big\} - \left\{\xi - \Delta_s^* B_s - \Delta_z^* A_z\right\}^2\Big] \qquad (28)$$

In this paper we have calculated the electrical conductivity, Peltier coefficient and electron thermal conductivity. We are interested in results in the axial direction, i.e. along the tubular axis. We noted that these paraemters are highly anisotropic, depending on the GCA θ_h, temperature T and the real overlapping integrals for jumps along the respective coordinates Δ_s and Δ_z.

We evaluated numerically the thermoelectric figure of merit Z defined by the relation $Z = \frac{\sigma \alpha^2}{\varkappa}$ where $\varkappa$ is the sum of the electron thermal conductivity $\varkappa_{zz}$ and lattice thermal conductivity $\varkappa_{lat}$

In most cases the dimensionless figure of merit ZT is used.

The thermopower α_{zz} obtained shows very interesting results, the details of which can be found in Figure 1. when Δz = 0.20 eV, 0.60 eV and 1.00 eV for Δs = 1.40 eV (Figure 1 (a)) or Δs = 1.80 eV (Figure 1 (b)), αzz 1/T , i.e., it exhibits semiconducting properties26

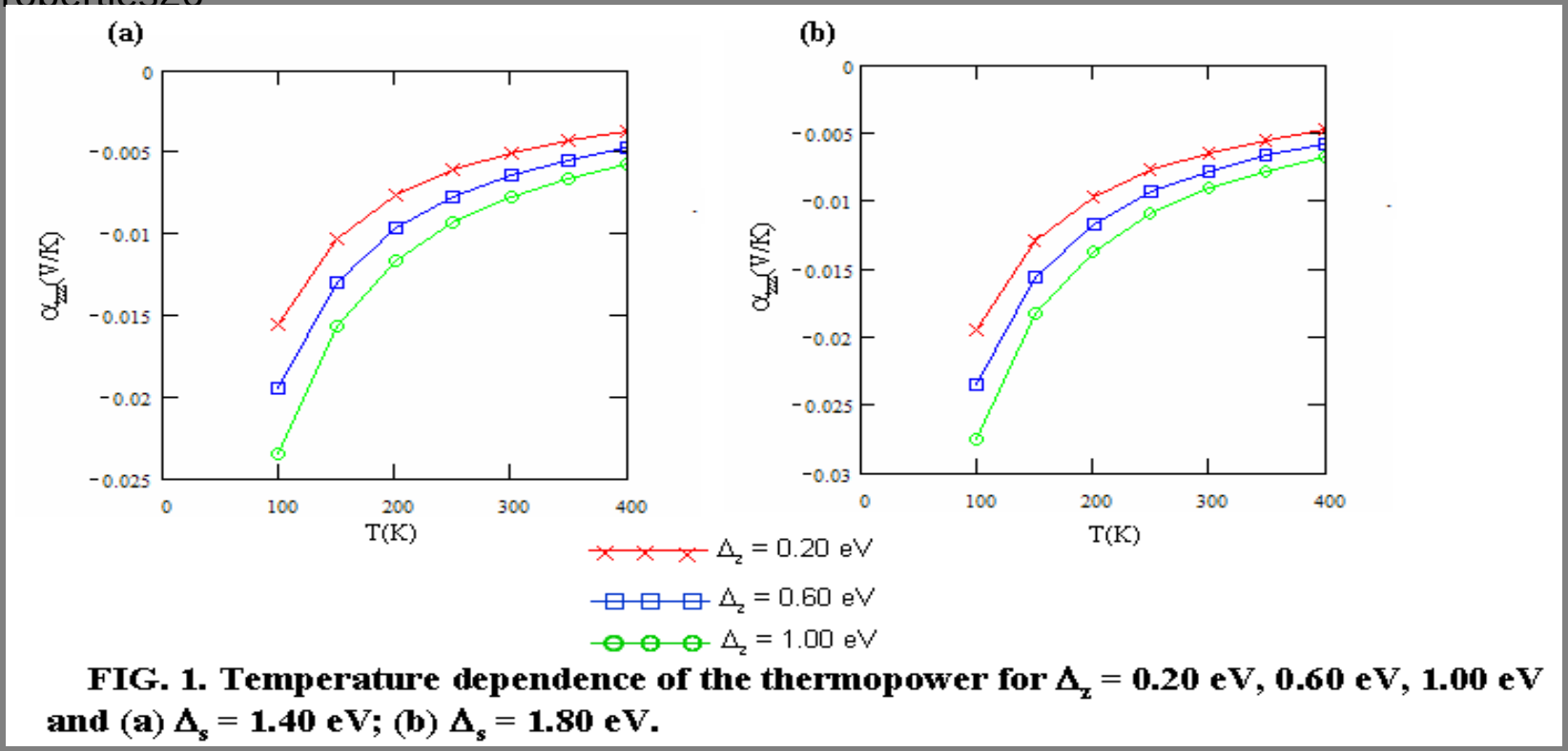

FIG. 1. Temperature dependence of the thermopower for Δ_z = 0.20 eV, 0.60 eV, 1.00 eV and (a) Δ_s = 1.40 eV; (b) Δ_s = 1.80 eV.

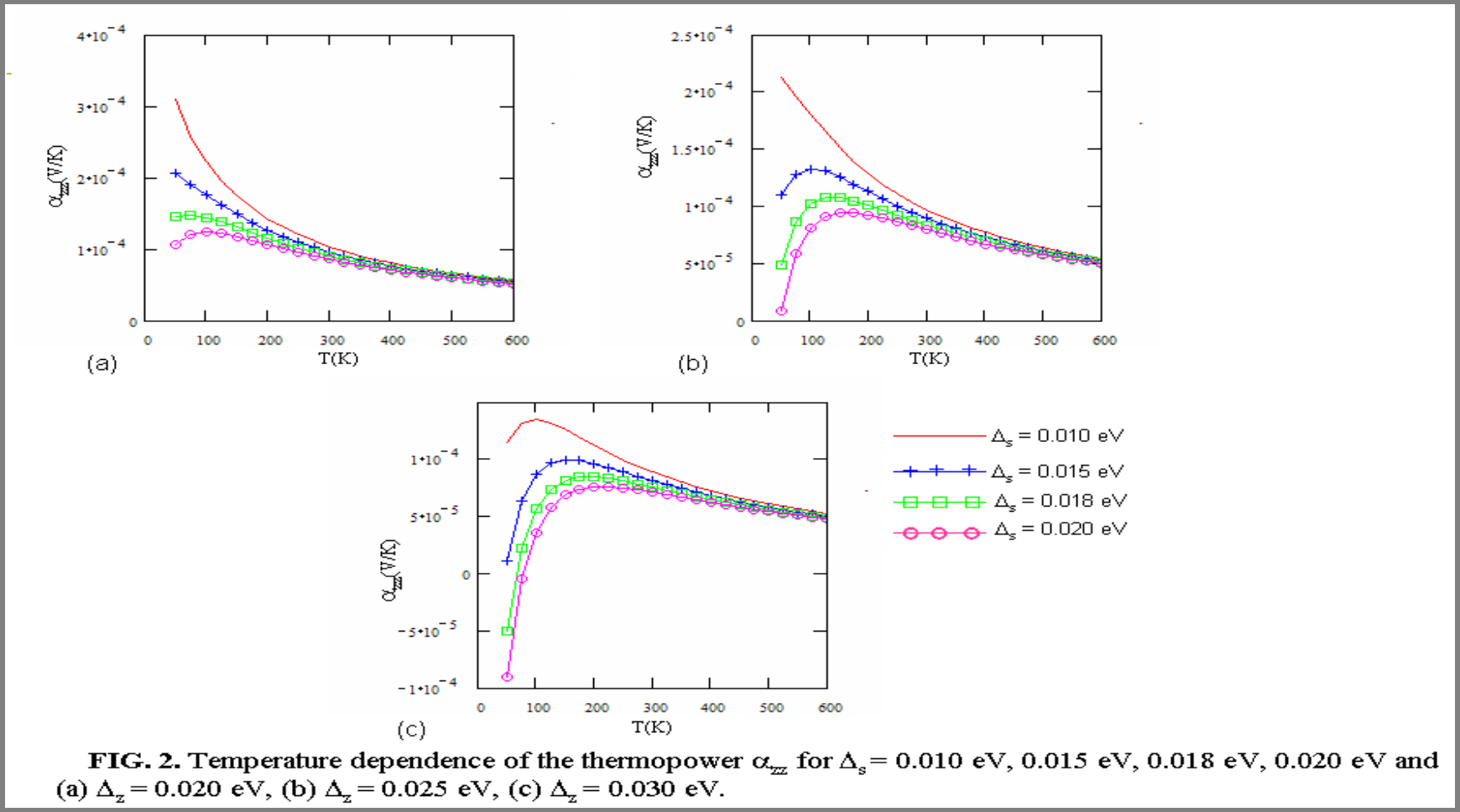

FIG. 2. Temperature dependence of the thermopower α_{zz} for $\Delta_s = 0.010$ eV, 0.015 eV, 0.018 eV, 0.020 eV and (a) $\Delta_z = 0.020$ eV, (b) $\Delta_z = 0.025$ eV, (c) $\Delta_z = 0.030$ eV.

However, when ∆s is varied from 0.010 eV to 0.020 eV keeping ∆z at 0.020 eV (Figure 2 (a)), 0.025 eV (Figure 2 (b)) and 0.030 eV (Figure 2 (c)), the thermopower αzz rises to a maximum value and then falls off. Such behaviour has been observed experimentally by Kong et al[18]. They attributed it to quasiparticle tunelling processes at some blockade sites. Also in[15] Grigorian et al observed this behaviour and attributed it to Kondo effect. But like Vavro and co-workers29 we attribute the phenomena to phonon drag effect which is important in doped SWNTs when electron-phonon scattering is the dominant decay mechanism for the phonons. We also observed that the peak value of αzz shifts between 100 K and 150 K as noted in[18].

With respect to the electron thermal conductivity κzz, we noted (Figure 3) that for values of Δz = 0.20 eV, 0.60 eV and 1.00 eV, and Δs = 1.40 eV or Δs = 1.80 eV, the electron thermal conductivity falls off monotonously. Particularly in Figure 3 (b), when

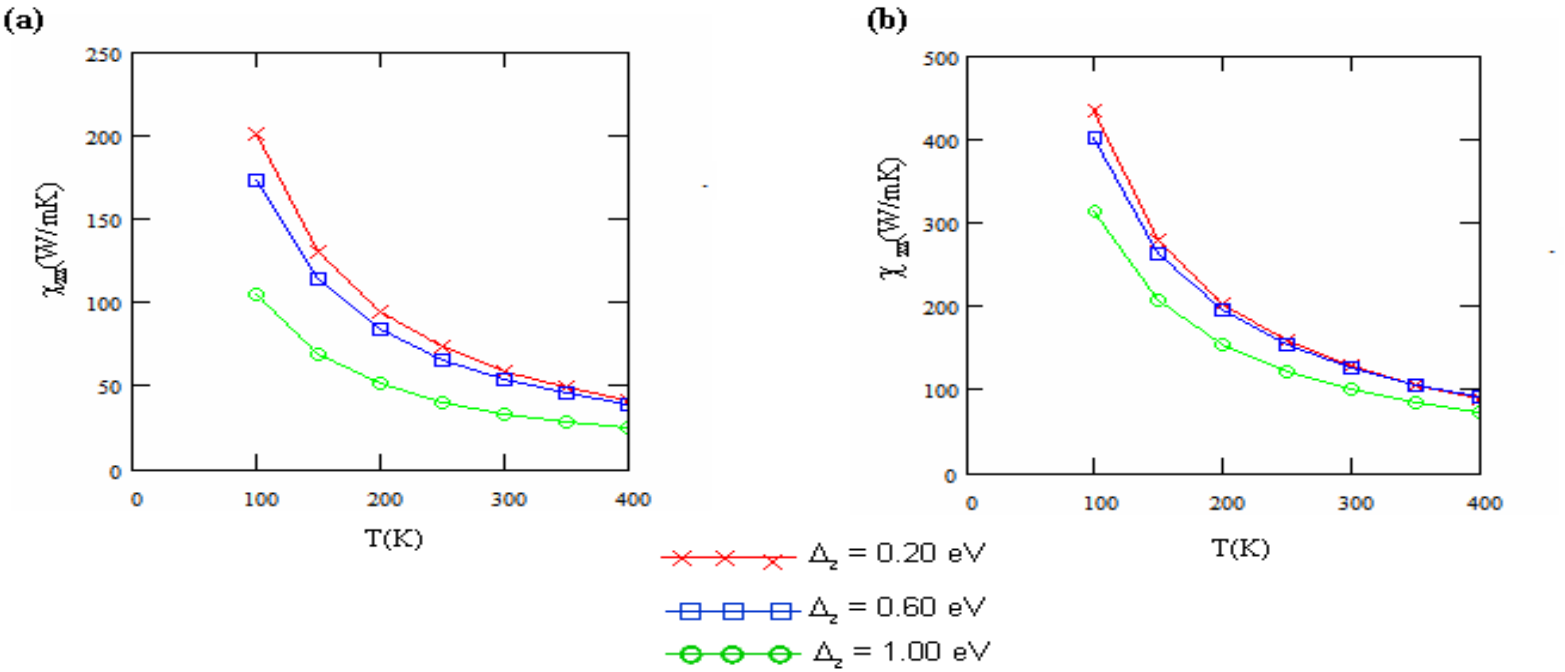

FIG. 3. Temperature dependence of the electron thermal conductivity χ_{zz} for $\Delta_z = 0.20$ eV, 0.60 eV, 1.00 eV and (a) $\Delta_s = 1.40$ eV; (b) $\Delta_s = 1.80$ eV

Δ_z = 0.6 eV and Δ_s = 1.80 eV, the κzz value at 100 K is around 400 W/mK and decreases to 200 W/mK at 400 K. A similar observation was made for the lattice thermal conductivity χ_{lat} of (5,5) SWNT with 40%—50% 14C impurity by Zhang et al.[31].

On the other hand when 0.010 eV≤ ∆s ≤ 0.020 eV and 0.020 eV≤ ∆z ≤ 0.030 eV (Figure 4), the electron thermal conductivity behaves in a similar manner as the lattice thermal conductivity obtained by Berber et al.19, i.e. the thermal conductivity rises to a maximum and then falls off. They exhibit unusually high thermal conductivity at around 100 K.

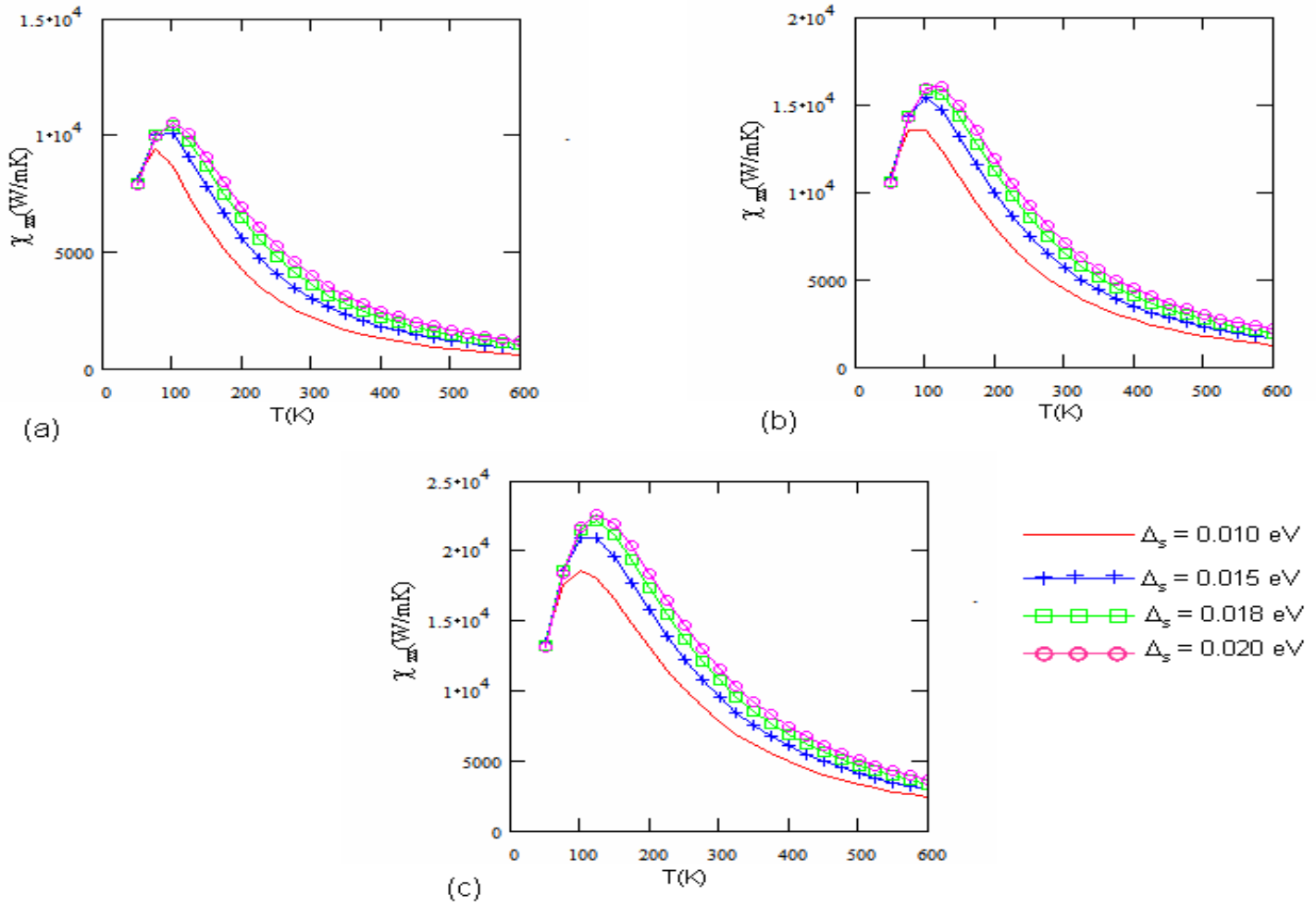

FIG. 4. Temperature dependence of the electron thermal conductivity χ_{zz} for Δ_s = 0.010 eV, 0.015 eV, 0.018 eV, 0.020 eV and (a) Δ_z = 0.020 eV, (b) Δ_z = 0.025 eV, (c) Δ_z = 0.030 eV.

To calculate the thermoelectric figure of merit, we needed to use lattice thermal conductivity data. Because of the similar behaviour of our curves to the curves of Zhang et al. and Berber et al., we calculated the thermoelectric figure of merit as a function of temperature using the lattice thermal conductivity data obtained by Zhang et al. for the case when 0.20 eV≤ $\Delta z \leq$ 1.00 eV and Δs = 1.40 eV and 1.80 eV, and by Berber et al. for the case when 0.010 eV≤ $\Delta s \leq$ 0.020 eV and 0.020 eV≤ $\Delta z \leq$ 0.030 eV.In fact in31 it was stated unambigously that unlike its electronic counterpart, the thermal conductivity of SWNTs does not depend on the chirality and/or atomic geometry sensitvely both at low temperature and room temperature. The results for case I), presented in Figure 5, shows that ZT could be greater than 1, and it decreases with both increasing temperature and Δz. However it increased slightly

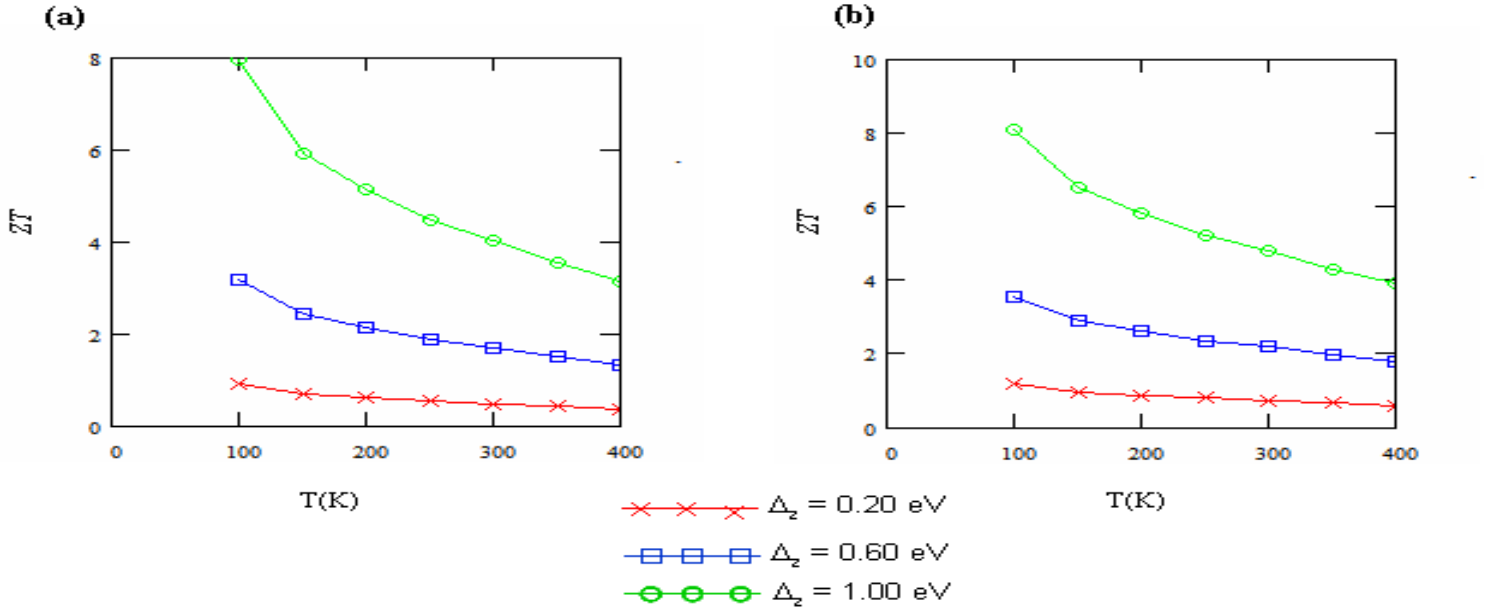

FIG. 5. Temperature dependence of the dimensionless thermoelectric figure of merit ZT for Δ_z = 0.20 eV, 0.60 eV, 1.00 eV and (a) Δ_s = 1.40 eV; (b) Δ_s = 1.80 eV

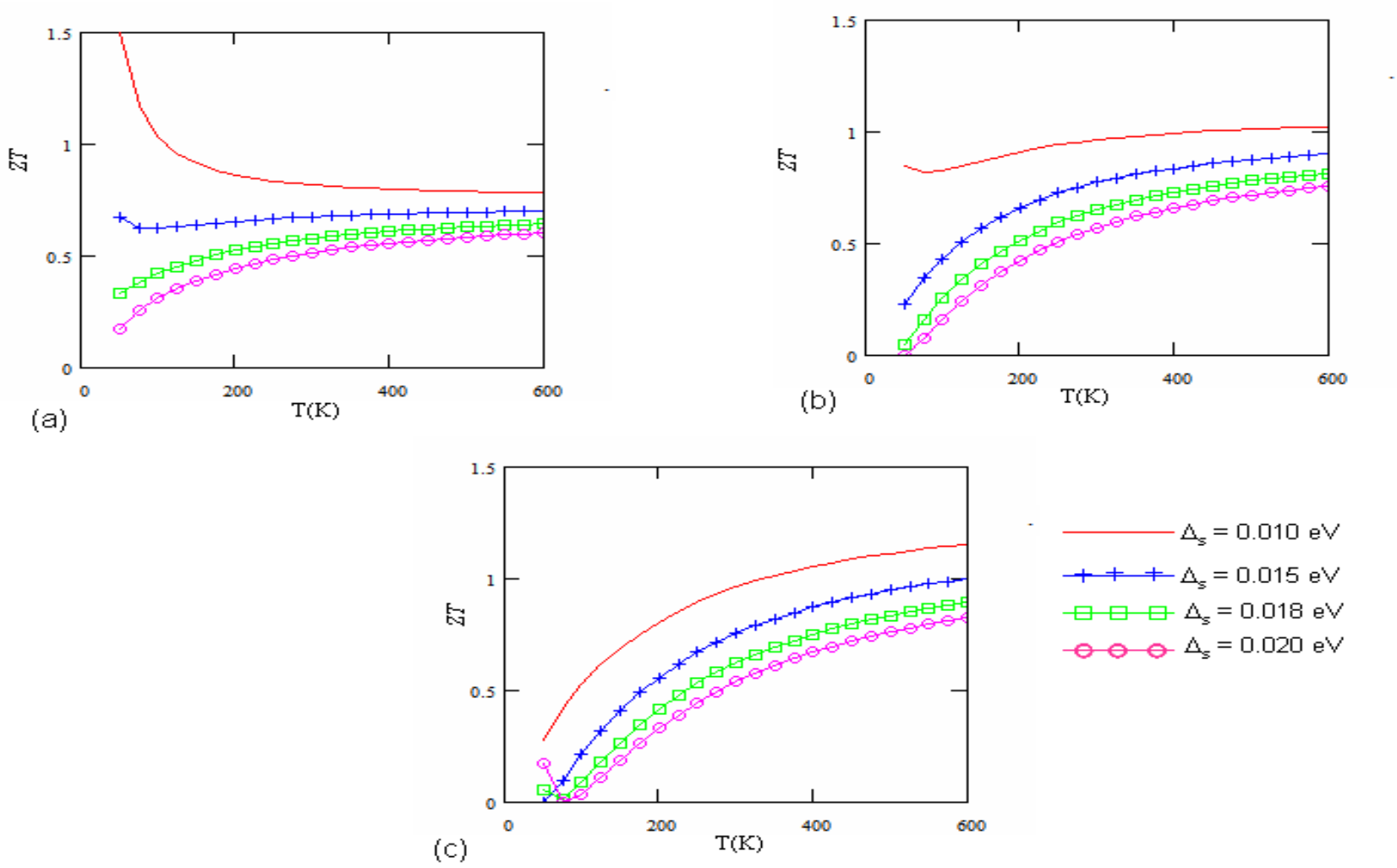

FIG. 6. Temperature dependence of *ZT* for Δ_s = 0.010 eV, 0.015 eV, 0.018 eV, 0.020 eV and (a) Δ_z = 0.020 eV, (b) Δ_z = 0.025 eV, (c) Δ_z = 0.030 eV.

when Δs was increased from 1.40 eV to 1.60 eV. For case II), it was observed (Figure 6) that for Δs = 0.010 eV and Δz = 0.020 eV, ZT is greater than 1 at low temperatures. It then falls rapidly with increasing T and attains a constant value of 0.8 at about 300 K. This result corroborates with the suggestion made by Small et al.30 which says that at temperatures below 30 K, ZT can be greater than 1 for single walled nanotubes (SWNTS). In that same paper it was suggested that ZT > 1 if $\alpha \sim 200\mu$ V/K. This also agrees with our results (see figs. (3a) and (3b)). On the other hand, as Δs changes from 0.018 eV to 0.020 eV at Δz = 0.020 eV, we observed that ZT is very small at low temperatures and increases with increasing temperature to a constant value. As can be seen from figs. (4b) and (4c) the behaviour of the graphs remain almost the same as we increase the values of Δz from 0.020 eV to 0.030 eV. However, we noted that ZT > 1 for values of Δs = 0.010 eV and Δz = 0.025 eV and 0.030 eV.

Conclusion: We have studied the thermoelectric effect of CNTs and noted that by optimizing T, Δz and Δs, ZT can be made greater than 1. This suggests that CNTs could be used as a thermoelement.

IMPACT FACTOR

Thermopower of carbon nanotubes in a magnetic field

N.G. Galkin, V.A. Margulis, and A.V. Shorokhov
Mordovian State University, 430000 Saransk, Russia

We investigate thermoelectric properties of single-wall nanotubes in a longitudinal magnetic field. To study the thermopower we use the approach in [1] together with model developed in [2]. We demonstrate that the thermopower dependence on the magnetic field and the electron energy has a spectrum of peaks. Additionally, the magnetic field splits the thermopower peaks. The manipulation of the magnetic field and other parameters of nanotubes can give rise to the giant thermopower. It is shown that the thermopower depends strongly on the nanotube radius. We stress that the thermopower dependence on temperature are in good qualitative agreement with experimental results [3] and theoretical ones [4] obtained in the tight-binding approximation with the help the Boltzmann kinetic equation.

The present work was supported by the Russian Ministry of Education (project N E02-3.4-370).

[1] P. Streda, *J.Phys.: Condens. Matter*, **1**, 1025 (1989).
[2] V.A. Geiler, V.A. Margulis, A.V. Shorokhov, *JETP*, **88**, 800 (1999).
[3] L. Grigorian, G.U. Sumanasekera, A.P. Loper, S.L. Fang, J.L. Allen, P.C. Eklund, *Phys.Rev. B*, **60**, R11 309 (1999).
[4] S.Y. Mensah, F.K.A. Allotey, N.G. Mensah, G. Nkrumah, *J.Phys.: Condens. Matter*, **13**, 5653 (2001).

IMPACT FACTOR

Electrical and thermal properties of carbon nanotube bulk materials: Experimental studies for the 328–958 K temperature range

Hai-Long Zhang,[1] Jing-Feng Li,[2,*] Bo-Ping Zhang,[1] Ke-Fu Yao,[3] Wei-Shu Liu,[1] and Heng Wang[2]
[1]*School of Materials Science and Engineering, University of Science and Technology Beijing, Beijing 100083, People's Republic of China*
[2]*State Key Laboratory of New Ceramics and Fine Processing, Department of Materials Science and Engineering, Tsinghua University, Beijing 100084, People's Republic of China*
[3]*Department of Mechanical Engineering, Tsinghua University, Beijing 100084, People's Republic of China*
(Received 19 August 2006; revised manuscript received 29 January 2007; published 3 May 2007)

We report on electrical and thermal properties in the temperature range from 328 to 958 K of multiwall carbon nanotube (MWNT) bulk materials that were consolidated by spark plasma sintering. The rather dense MWNT bulk materials show exclusively nonmetallic temperature dependence of electrical conductivity from 328 to 958 K, owing to the absence of metallic conduction mechanism in such a highly disordered system. The conductivity exhibited extremely weak temperature dependence with only 35% increase of room-temperature conductivity at 958 K, which was explained by a heterogeneous model considering both fluctuation-assisted tunneling between nanotubes or shells of MWNT and variable-range hopping between graphite microphases that were observed to be dispersed in MWNT bulk materials. The results suggest that fluctuation-assisted tunneling governed this weak conductivity-temperature dependence. Metallic diffusion behavior was observed from 328 to 958 K, and it indicates that phonon drag contributed little to the thermoelectric power of MWNT bulk materials. By contrast, we further show that the increase in sample dimensionality from individual MWNT to bulk materials tends to increase the metallic temperature dependence of electrical conductivity and remarkably decrease the magnitude of thermal conductivity. The geometric shift from graphene sheet to tubular nanotube for carbon-related bulk materials changes the conduction from the combination of *n* and *p* types to absolute *p* type.

DOI: 10.1103/PhysRevB.75.205407 PACS number(s): 73.63.−b, 73.50.Lw, 65.80.+n, 81.07.De

IMPACT FACTOR

Mensah *et al.*[30] theoretically predicted that carbon nanotubes may serve as a good thermoelectric material. So we also evaluate the thermoelectric properties of our MWNT bulk materials in this study. Figure 9 shows the thermoelectric figure of merit Z of MWNT bulk materials as a function of temperature. The value of Z was calculated by

$$Z = S^2\sigma/k. \qquad (5)$$

[30] S. Y. Mensah, F. K. A. Allotey, N. G. Mensah, and G. Nkrumah, J. Phys.: Condens. Matter **13**, 5653 (2001).

[31] C. Qin, X. Shi, S. Q. Bai, L. D. Chen, and L. J. Wang, Mater. Sci.

Thermal rectification in carbon nanotube intramolecular junctions: Molecular dynamics calculations

Gang Wu*

Department of Physics and Centre for Computational Science and Engineering, National University of Singapore, Singapore 117542-76, Republic of Singapore

Baowen Li†

Department of Physics and Centre for Computational Science and Engineering, National University of Singapore, Singapore 117542-76, Republic of Singapore and NUS Graduate School for Integrative Sciences and Engineering, Singapore 117597, Republic of Singapore

(Dated: July 28, 2007)

We study heat conduction in $(n, 0)/(2n, 0)$ intramolecular junctions by using molecular dynamics method. It is found that the heat conduction is asymmetric, namely, heat transports preferably in one direction. This phenomenon is also called thermal rectification. The rectification is weakly dependent on the detailed structure of connection part, but is strongly dependent on the temperature gradient. We also study the effect of the tube radius and intramolecular junction length on the rectification. Our study shows that the tensile stress can increase rectification. The physical mechanism of the rectification is explained.

PACS numbers: 66.70.+f, 44.10.+i, 61.46.Fg, 65.80.+n

IMPACT FACTOR

On the other hand, there have been increasing studies on heat conduction in real nano scale systems[8]. For example, the thermal conduction of single walled carbon nanotubes (SWCNTs) has attracted both theoretical[9,10,11,12,13,14,15,16,17,18] and experimental[19,20,21,22,23,24,25] attentions. Almost all experiments and numerical simulations have payed their attention to the extremely high thermal conductivity of SWCNTs. The dependence of the thermal conductiv-

[10] S. Maruyama, Physica B **323**, 193 (2002); S. Maruyama, Microscale Thermophysical Engineering **7**, 41 (2003).

[11] W. Zhang, Z.Y. Zhu, F. Wang, T.T. Wang, L.T. Sun, and Z.X. Wang, Nanotechnology **15**, 936 (2004).

[12] N.G. Mensah, G. Nkrumah, S.Y. Mensah, and F.K.A. Allotey, Phys. Lett. A **329**, 369 (2004).

[13] Z. Yao, J.S. Wang, B. Li, and G.R. Liu, Phys. Rev. B **71**, 085417 (2005).

IMPACT FACTOR

High thermal conductivity of carbon nanotube reinforced copper materials

Guangyu Chai and Quanfang Chen*

MEMS and Nanomaterials Lab, Mechanical, Materials and Aerospace Engineering Department, University of Central Florida

Orlando, FL 32816-2450. *qchen@mail.ucf.edu

IMPACT FACTOR

Carbon nanotubes (CNT) [1-3] have attracted more and more research interests for their excellent properties and various potential applications. Theoretical studies show that the thermal conductivity of a single-walled carbon nanotube (SWNT) at room temperature is about 6,600 W/m.K [4] to 11,000 W/m.K [5]. The measured thermal conductivity is as high as 7,000 W/m-K [6] for a SWNT, and 3000 W/m-k [7] for a multi-walled carbon nanotube (MWNT) respectively. These thermal conductivity values are essentially higher than that of diamond. Therefore, these remarkable thermal

4. S. Berber, Y-K. Kwon, and D. Tomanek, Unusually high thermal conductivity of carbon nanotubes, Physical Review Letters 84 No. 20 (2000) 4613-4616.
5. S.Y. Mensah, F.K.A. Allotey, G. Nkrumah, N.G. Mensah, High electron thermal conductivity of chiral carbon nanotubes, Physica E 23 (2004) 152-158

IMPACT FACTOR

Физика и техника полупроводников, 2009, том 43, вып. 4

Термоэлектродвижущая сила углеродных нанотрубок

© А.В. Мавринский¶, Е.М. Байтингер

Челябинский государственный педагогический университет,
454080 Челябинск, Россия

(Получена 12 декабря 2007 г. Принята к печати 21 мая 2008 г.)

Представлены результаты расчетов температурной зависимости коэффициента термоэдс графита и полуметаллических углеродных нанотрубок с учетом цилиндричности их надатомного строения. Использованы уравнение Больцмана и π-электронная модель полуметаллических углеродных нанотрубок. Основными параметрами расчета являлись: концентрация электронов, энергия Ферми и энергия локального уровня, обусловленного цилиндричностью углеродных нанотрубок. Результаты расчетов сопоставляются с известными экспериментальными данными.

PACS: 72.15.Jf, 73.63.Fg

1. Введение

Углеродные нанотрубки, впервые синтезированные Ижимой в 1991 году [1], относятся к классу графитоподобных материалов. Имеется ряд уникальных свойств, которые унаследовали нанотрубки от графита, — высокая термическая стойкость, низкий коэффициент термического расширения и др. Однако особое каркасное строение цилиндрической формы придает нанотрубкам свойства, часто существенно отличающие их от графита. В первую очередь это относится к электронным свой-

строения образующего их монослоя графита, часто называемого графеновым листом. Зонная структура монослоя относительно проста [7]. Графеновый лист является двумерным полуметаллом: валентная зона и зона проводимости π-электронов соприкасаются. При наличии соседних графитовых слоев (в случае объемного образца) происходит небольшое перекрывание энергетических зон, так что равновесная концентрация свободных π-электронов (и дырок) при комнатной температуре составляет незначительную величину, $\sim 10^{18}$ см$^{-3}$. Высокая электропроводность графита обусловлена исклю-

Как показано в [6], углеродные нанотрубки вполне могут быть подходящим материалом для создания эффективных термоэлектрических преобразователей. Дан-

трубок основаны разрабатываемые химические сенсоры газов [5].

Как показано в [6], углеродные нанотрубки вполне могут быть подходящим материалом для создания эффективных термоэлектрических преобразователей. Данная статья представляет развитие этого научного направления. Она состоит из краткого описания зонного строения нанотрубок в сопоставлении с аналогичным зонным строением графитового слоя, описания метода расчетов коэффициента термоэлектродвижущей силы графита и нанотрубок, сопоставления результатов с экспериментом и обсуждения.

2. Электронное строение графенового листа

Для описания термоэлектрических характеристик углеродных нанотрубок необходимо знание электронного

¶ E-mail: mavrinsky@gmail.com

луэмпирическом методе сильной связи), $\chi = k - k_0$ — волновое число π-электронов. Знаки ($\pm$) означают, что π-зоны зеркальны в небольшой окрестности точки их касания.

С учетом (1) плотность состояний определяется как (графически представлена на вставке к рис. 1)

$$N(E) = B\,|E|, \tag{2}$$

где

$$B = \frac{16}{3\pi\gamma_0^2 b^2 c}. \tag{3}$$

Коэффициент пропорциональности B линейной зависимости плотности состояний π-электронов от энергии $N(E)$, как видно из формулы (3), определяется еще и параметром c — периодом элементарной ячейки в перпендикулярном слою направлении. Для идеального кристалла графита $c = 0.67$ нм. Введение этого параметра в (2) обусловлено необходимостью сравнивать расчеты с экспериментальными результатами, получаемыми

IMPACT FACTOR

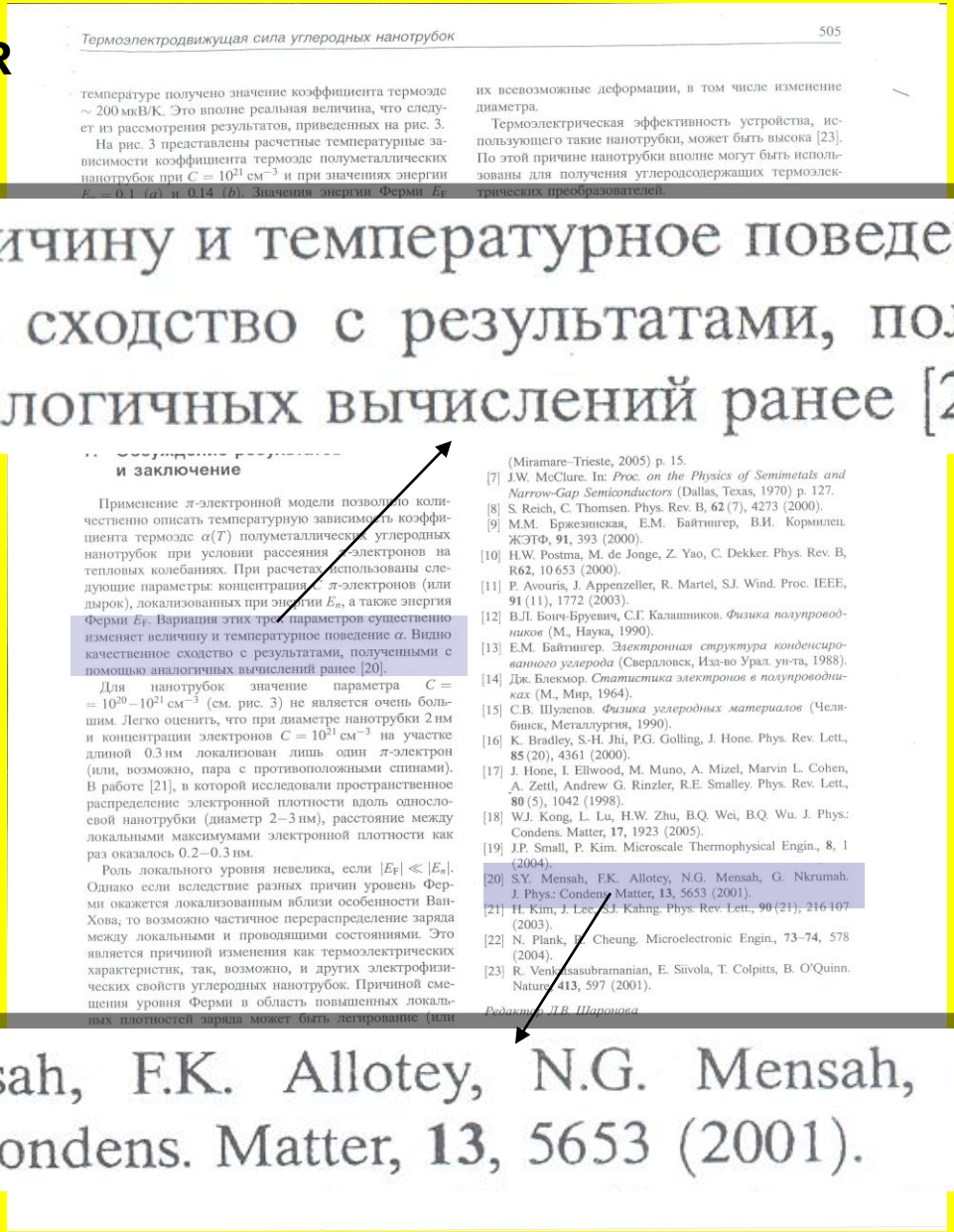

Термоэлектродвижущая сила углеродных нанотрубок 505

температуре получено значение коэффициента термоэдс ~ 200 мкВ/К. Это вполне реальная величина, что следует из рассмотрения результатов, приведенных на рис. 3.

На рис. 3 представлены расчетные температурные зависимости коэффициента термоэдс полуметаллических нанотрубок при $C = 10^{21}$ см$^{-3}$ и при значениях энергии $E_n = 0.1$ (*a*) и 0.14 (*b*). Значения энергии Ферми E_F

их всевозможные деформации, в том числе изменение диаметра.

Термоэлектрическая эффективность устройства, использующего такие нанотрубки, может быть высока [23]. По этой причине нанотрубки вполне могут быть использованы для получения углеродсодержащих термоэлектрических преобразователей.

изменяет величину и температурное поведение α. Видно качественное сходство с результатами, полученными с помощью аналогичных вычислений ранее [20].

и заключение

Применение π-электронной модели позволило количественно описать температурную зависимость коэффициента термоэдс $\alpha(T)$ полуметаллических углеродных нанотрубок при условии рассеяния π-электронов на тепловых колебаниях. При расчетах использованы следующие параметры: концентрация C π-электронов (или дырок), локализованных при энергии E_n, а также энергия Ферми E_F. Вариация этих трех параметров существенно изменяет величину и температурное поведение α. Видно качественное сходство с результатами, полученными с помощью аналогичных вычислений ранее [20].

Для нанотрубок значение параметра $C = 10^{20}-10^{21}$ см$^{-3}$ (см. рис. 3) не является очень большим. Легко оценить, что при диаметре нанотрубки 2 нм и концентрации электронов $C = 10^{21}$ см$^{-3}$ на участке длиной 0.3 нм локализован лишь один π-электрон (или, возможно, пара с противоположными спинами). В работе [21], в которой исследовали пространственное распределение электронной плотности вдоль однослоевой нанотрубки (диаметр 2–3 нм), расстояние между локальными максимумами электронной плотности как раз оказалось 0.2–0.3 нм.

Роль локального уровня невелика, если $|E_F| \ll |E_n|$. Однако если вследствие разных причин уровень Ферми окажется локализованным вблизи особенности Ван-Хова, то возможно частичное перераспределение заряда между локальными и проводящими состояниями. Это является причиной изменения как термоэлектрических характеристик, так, возможно, и других электрофизических свойств углеродных нанотрубок. Причиной смещения уровня Ферми в область повышенных локальных плотностей заряда может быть легирование (или

(Miramare–Trieste, 2005) p. 15.
[7] J.W. McClure. In: *Proc. on the Physics of Semimetals and Narrow-Gap Semiconductors* (Dallas, Texas, 1970) p. 127.
[8] S. Reich, C. Thomsen. Phys. Rev. B, **62** (7), 4273 (2000).
[9] М.М. Бржезинская, Е.М. Байтингер, В.И. Кормилец. ЖЭТФ, **91**, 393 (2000).
[10] H.W. Postma, M. de Jonge, Z. Yao, C. Dekker. Phys. Rev. B, **R62**, 10 653 (2000).
[11] P. Avouris, J. Appenzeller, R. Martel, S.J. Wind. Proc. IEEE, **91** (11), 1772 (2003).
[12] В.Л. Бонч-Бруевич, С.Г. Калашников. *Физика полупроводников* (М., Наука, 1990).
[13] Е.М. Байтингер. *Электронная структура конденсированного углерода* (Свердловск, Изд-во Урал. ун-та, 1988).
[14] Дж. Блекмор. *Статистика электронов в полупроводниках* (М., Мир, 1964).
[15] С.В. Шулепов. *Физика углеродных материалов* (Челябинск, Металлургия, 1990).
[16] K. Bradley, S.-H. Jhi, P.G. Golling, J. Hone. Phys. Rev. Lett., **85** (20), 4361 (2000).
[17] J. Hone, I. Ellwood, M. Muno, A. Mizel, Marvin L. Cohen, A. Zettl, Andrew G. Rinzler, R.E. Smalley. Phys. Rev. Lett., **80** (5), 1042 (1998).
[18] W.J. Kong, L. Lu, H.W. Zhu, B.Q. Wei, B.Q. Wu. J. Phys.: Condens. Matter, **17**, 1923 (2005).
[19] J.P. Small, P. Kim. Microscale Thermophysical Engin., **8**, 1 (2004).
[20] S.Y. Mensah, F.K. Allotey, N.G. Mensah, G. Nkrumah. J. Phys.: Condens. Matter, **13**, 5653 (2001).
[21] H. Kim, J. Lee, S.J. Kahng. Phys. Rev. Lett., **90** (21), 216 107 (2003).
[22] N. Plank, P. Cheung. Microelectronic Engin., **73–74**, 578 (2004).
[23] R. Venkatasubramanian, E. Siivola, T. Colpitts, B. O'Quinn. Nature, **413**, 597 (2001).

Редактор Л.В. Шаронова

[20] S.Y. Mensah, F.K. Allotey, N.G. Mensah, G. Nkrumah. J. Phys.: Condens. Matter, **13**, 5653 (2001).

IMPACT FACTOR

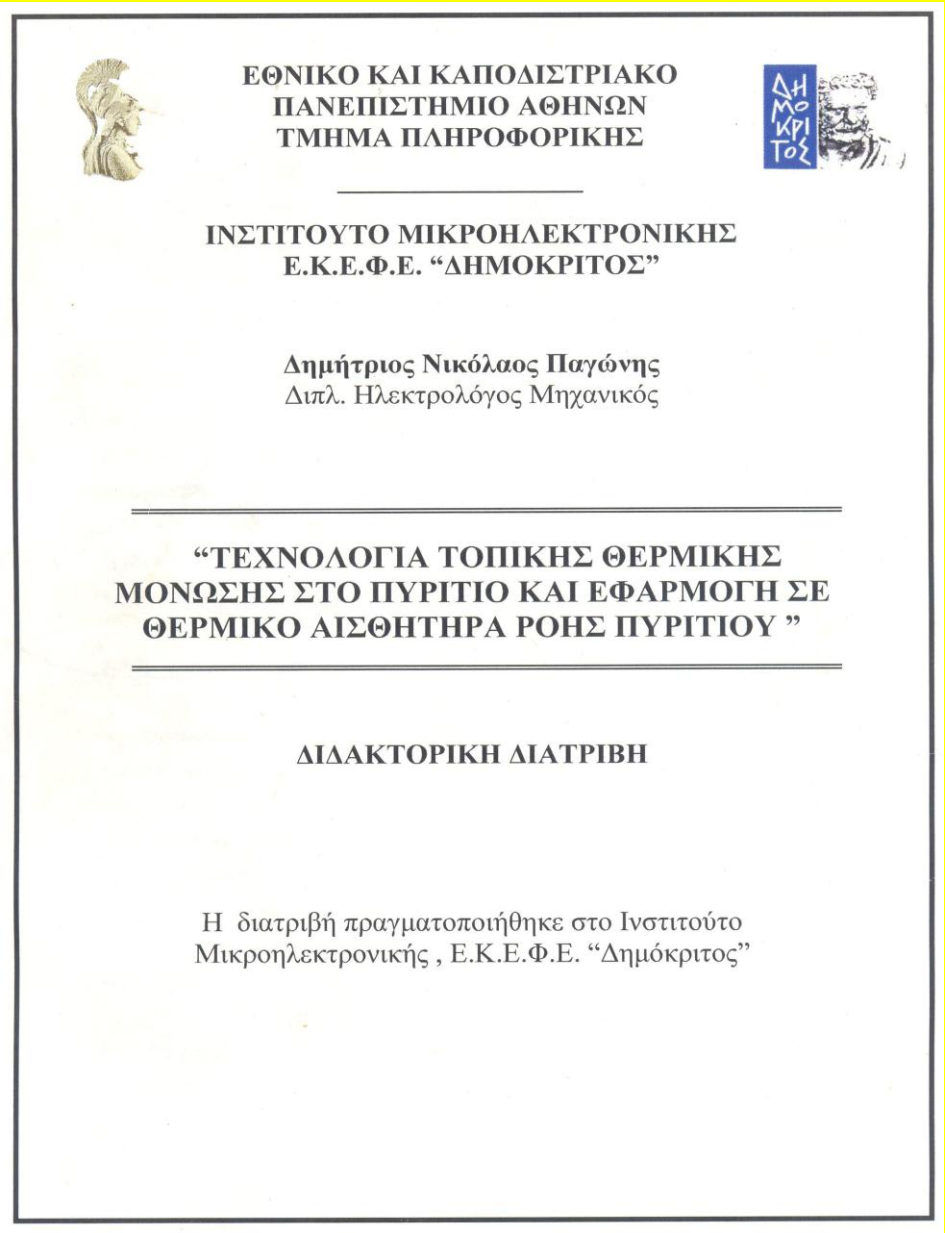

ΕΘΝΙΚΟ ΚΑΙ ΚΑΠΟΔΙΣΤΡΙΑΚΟ
ΠΑΝΕΠΙΣΤΗΜΙΟ ΑΘΗΝΩΝ
ΤΜΗΜΑ ΠΛΗΡΟΦΟΡΙΚΗΣ

ΙΝΣΤΙΤΟΥΤΟ ΜΙΚΡΟΗΛΕΚΤΡΟΝΙΚΗΣ
Ε.Κ.Ε.Φ.Ε. "ΔΗΜΟΚΡΙΤΟΣ"

Δημήτριος Νικόλαος Παγώνης
Διπλ. Ηλεκτρολόγος Μηχανικός

"ΤΕΧΝΟΛΟΓΙΑ ΤΟΠΙΚΗΣ ΘΕΡΜΙΚΗΣ ΜΟΝΩΣΗΣ ΣΤΟ ΠΥΡΙΤΙΟ ΚΑΙ ΕΦΑΡΜΟΓΗ ΣΕ ΘΕΡΜΙΚΟ ΑΙΣΘΗΤΗΡΑ ΡΟΗΣ ΠΥΡΙΤΙΟΥ "

ΔΙΔΑΚΤΟΡΙΚΗ ΔΙΑΤΡΙΒΗ

Η διατριβή πραγματοποιήθηκε στο Ινστιτούτο Μικροηλεκτρονικής , Ε.Κ.Ε.Φ.Ε. "Δημόκριτος"

IMPACT FACTOR

απόσβεσης υπό μεγάλη πίεση με συγκεκριμένο ρυθμό ψύξης ("…by quenching melted Pb-Sn-Te powders within a certain pressure range at a given cooling rate…") [77]. Το μέγεθος κόκκου (grain size) του σχηματισμένου κράματος μετρήθηκε με τεχνική μικροσκοπίας και είναι λιγότερο από 100 νανόμετρα(σχήμα 2.3.3.β).

Οι S.Y.Mensah et al [78], προτείνουν ένα θεωρητικό μοντέλο πρόβλεψης του συντελεστή Seebeck για νανοσωλήνες άνθρακα (Carbon Nanotybes, CNTs). Μέσω του συγκεκριμένου μοντέλου, παρατήρησαν ότι το συγκεκριμένο υλικό μπορεί να συμπεριφερθεί είτε ως ημιαγωγός π-τύπου είτε ως ν-τύπου ανάλογα με τις παραμέτρους παρασκευής του. Οι προβλεπόμενες τιμές του συντελεστή Seebeck για την περίπτωση που το υλικό συμπεριφέρεται ως ν-τύπου ημιαγωγός (η πλειοψηφία των φορέων είναι οπές) είναι από -4000 έως -500 μV/K ενώ για την περίπτωση που συμπεριφέρεται ως π-τύπου (η πλειοψηφία των φορέων αποτελείται από ηλεκτρόνια) είναι από 50 έως 100 μV/K .

Συγκρίνοντας τις αναφερόμενες τιμές συντελεστή Seebeck και στις τρεις περιπτώσεις, με τις υπάρχουσες για τα "συμβατικά υλικά", μπορούμε να

Οι S.Y.Mensah et al [78], προτείνουν ένα θεωρητικό μοντέλο πρόβλεψης του συντελεστή Seebeck για νανοσωλήνες άνθρακα (Carbon Nanotybes, CNTs). Μέσω του συγκεκριμένου μοντέλου, παρατήρησαν ότι το συγκεκριμένο υλικό μπορεί

δείκτη απόδοσης αποτελεί η εξασφάλιση όσο το δυνατόν μεγαλύτερης θερμοκρασιακής διαφοράς μεταξύ των δύο περιοχών (ψυχρής και θερμής) και χαμηλής θερμικής χωρητικότητας των θερμοζευγών (για την εξασφάλιση γρήγορης απόκρισης) [83].

Οι M.Strasser et al [79], δημοσίευσαν σχετικά πρόσφατα (2000) μια πιθανή διάταξη μίας θερμοηλεκτρικής γεννήτριας χαμηλής ισχύος. Τα θερμοζεύγη που προτείνουν αποτελούνται από πολυκρυσταλλικό πυρίτιο - γερμάνιο (poly-$Si_{70\%}Ge_{30\%}$) ενώ η θερμική μόνωση προσφέρεται μέσω μικρομηχανικής όγκου και συγκεκριμένα μέσω ενός θυσιαζόμενου επιπέδου διοξειδίου του πυριτίου. Σύμφωνα με κατάλληλες θεωρητικές προσομοιώσεις από τους ίδιους ερευνητές, για μία θερμοκρασιακή

IMPACT FACTOR

Available online at www.sciencedirect.com
SCIENCE DIRECT
Carbon 44 (2006) 710–717
CARBON
www.elsevier.com/locate/carbon

Evaluation of effective thermal conductivity for carbon nanotube/polymer composites using control volume finite element method

Young Seok Song, Jae Ryoun Youn *

School of Materials Science and Engineering, Seoul National University, 56-1, Shinlim-Dong, Gwanak-Gu, Seoul, 151-744 Republic of Korea

Received 27 May 2005; accepted 21 September 2005
Available online 9 November 2005

ments have been carried out to measure thermal conductivities of the single walled carbon nanotube (SWNT) and the multiwalled carbon nanotube (MWNT) [5–7]. However, the measured thermal conductivity varied drastically from 30 to 3000 W/m K. Moreover, some of the thermal conductivities calculated based on the molecular dynamics (MD) simulation were as high as 6000 W/m K at room temperature for an isolated SWNT [8–10]. On the other hand, it is known that carbon fiber and carbon fiber reinforced carbon/carbon (CC) composites have thermal

[8] Berber S, Kwon YK, Tománek D. Unusually high thermal conductivity of carbon nanotubes. Phys Rev Lett 2000;8:4:4613–6.
[9] Che J, Cadin, Goddard III WA. Thermal conductivity of carbon nanotubes. Nanotechnology 2000;11:65–9.
[10] Mensah NG, Nkrumah G, Mensah SY, Allotey FKA. Temperature dependence of the thermal conductivity in chiral carbon nanotubes. Phys Lett A 2004;329:369–78.

ScienceDirect
makes sense.
http://www.sciencedirect.com/

Top 25 Hottest Articles

Physics and Astronomy > Physics Letters A
July - September 2004

RSS | Blog This! | Articles in Press | Print | Show condensed

P. Holland

1. **Thermal and electrical transport in multi-walled carbon nanotubes** • Short communication
   Physics Letters A, Volume 329, Issue 3, 23 August 2004, Pages 207–213
   D.J. Yang, S.G. Wang, Q. Zhang, P.J. Sellin, G. Chen
2. **Mechanism of finite-amplitude double-component convection due to different boundary conditions** • Short communication
   Physics Letters A, Volume 329, Issue 6, 6 September 2004, Pages 445–450
   N. Tsitverblit
3. **Jean-Pierre Vigier 1920@?-@?2004**
   Physics Letters A, Volume 328, Issue 6, 9 August 2004, Pages 417–418
4. **Temperature dependence of the thermal conductivity in chiral carbon nanotubes** • Short communication
   Physics Letters A, Volume 329, Issue 4–5, 30 August 2004, Pages 369–378
   N.G. Mensah, G. Nkrumah, S.Y. Mensah, F.K.A. Allotey
5. **Global robust asymptotical stability of multi-delayed interval neural networks:** • Short communication
   Physics Letters A, Volume 328, Issue 6, 9 August 2004, Pages 452–462
   C. Li, X. Liao, R. Zhang
6. **Nonclassical properties of coherent states** • Short communication
   Physics Letters A, Volume 329, Issue 3, 23 August 2004, Pages 184–187
   L.M. Johansen
7. **Quantum dialogue** • Short communication

THANK YOU

ALL SOO MUCH!